THESIS FOR THE DEGREE OF DOCTOR OF PHILOSOPHY

Modelling of laser plasma interaction with applications to particle acceleration and radiation generation

BENJAMIN SVEDUNG WETTERVIK

Department of Physics

CHALMERS UNIVERSITY OF TECHNOLOGY

Gothenburg, Sweden 2019

Modelling of laser plasma interaction with applications to particle acceleration and radiation generation
BENJAMIN SVEDUNG WETTERVIK
ISBN 978-91-7905-152-5

Doktorsavhandlingar vid Chalmers tekniska högskola
Ny series nr 4619
ISSN 0346-718X

Department of Physics
Chalmers University of Technology
SE-412 96 Göteborg
Sweden
Tel: +46 (0) 31 772 1000

Printed in Sweden by
Reproservice
Chalmers Tekniska Högskola
Göteborg, Sweden, 2019

Modelling of laser plasma interaction with applications to particle acceleration and radiation generation

Benjamin Svedung Wettervik
Department of Physics
Chalmers University of Technology

Abstract

The development of laser systems with ultra-high intensities has allowed the study of the relativistic interaction of laser light and ionized matter, plasmas, as well as opened up prospects for compact particle accelerators, generation of high intensity X-ray, XUV radiation, and probing QED-effects, which are present in the high intensity regime. To describe laser matter interaction, it is necessary to self-consistently account for the paths of a large number of particles and the corresponding electromagnetic fields, with the addition of stochastic effects at high laser intensities. Although analytical work can capture the essence of the dynamics in a range of situations, the rich dynamics in laser-plasma interaction results in that numerical modelling, and in particular the Particle-In-Cell (PIC) method, is critical to gain a detailed description of the dynamics. This is a stochastic method in which phase-space is sampled with macro-particles and allows for efficient modelling of high dimensional problems, but has limitations due to statistical noise.

For some applications, for example shock acceleration and instability growth, continuum methods, i.e. solving the Vlasov-Maxwell system of equations on a phase-space grid, may be preferable to accurately describe the plasma dynamics. In the first two papers in this thesis, we address the problem of implementing efficient continuum methods for the Vlasov-Maxwell system of equations. Furthermore, we treat ion shock acceleration using continuum methods. In the following papers, we address scalings of the electron spectrum in the electron sheath, formed at the vacuum-plasma boundary through the interaction of a relativistic laser and moderately overdense plasma. This is important to determine the spectral properties of high harmonic radiation generated from the laser plasma interaction. We also explore electron wakefield acceleration driven by laser pulses with wavelength in the X-ray regime generated from laser plasma interaction in the moderately overdense regime. By reducing the wavelength, the quantum parameter χ is enhanced, leading to comparable electron and photon energies already at moderate relativistic amplitudes although with more infrequent emission of photons than at optical wavelengths, preventing radiation losses from becoming a roadblock for the acceleration process.

Keywords: plasma, Vlasov-Maxwell equations, continuum methods, ion acceleration, coherent X-ray pulses, electron wakefield acceleration, radiation generation

Publications

This thesis is based on the following publications:

A B. Svedung Wettervik, T. C. DuBois and T. Fülöp,
Vlasov modelling of laser-driven collisionless shock acceleration of protons,
Physics of Plasmas 23, 053103, 2016.
arXiv:1512.06644 [physics.plasm-ph]

B B. Svedung Wettervik, T. C. DuBois, E. Siminos and T. Fülöp,
Relativistic Vlasov-Maxwell modelling using finite volumes and adaptive mesh refinement,
The European Physical Journal D 71 (6), 157, 2017.
arXiv:1606.08681 [physics.plasm-ph]

C B. Svedung Wettervik, A. Gonoskov, and M. Marklund,
Prospects and limitations of wakefield acceleration in solids,
Physics of Plasmas 25, 013107, 2018.
arXiv:1709.02190 [physics.plasm-ph]

D B. Svedung Wettervik, M. Marklund, and A. Gonoskov,
Physics of the laser-plasma interface in the relativistic regime of interaction,
Physics of Plasmas 26, 053101, 2019.
arXiv:1901.04175 [physics.plasm-ph]

Other publications, not included in the thesis:

E E. Siminos, M. Grech, B. Svedung Wettervik and T. Fülöp, *Kinetic and finite ion mass effects on the transition to relativistic self-induced transparency in laser-driven ion acceleration,* New Journal of Physics 19 (12), 123042, 2017. arXiv:1603.06436 [physics.plasm-ph]

Statement of contribution

Paper A

Vlasov modelling of laser-driven collisionless shock acceleration of protons

In this paper, we implement and use continuum methods to solve the Vlasov-Maxwell system of equations in two dimensions (one spatial and momentum dimension). We investigate the interaction between the TNSA and shock acceleration mechanisms. In particular we study the effect of using a layered target, where the shock is launched in a front layer with light ions and then continues through a heavy ion backside. This leads to a removal of the pure TNSA contribution to the spectrum and increases the energy of the shock accelerated ions slightly.

I was responsible for the development of the code, suggesting the setups to be studied as well as running the simulations. The results were analyzed by me, in collaboration with my co-authors, followed by me preparing the draft of the paper. The draft was then finalized together with my co-authors.

Paper B

Relativistic Vlasov-Maxwell modelling using finite volumes and adaptive mesh refinement

In this paper, we present a block structured adaptive finite volume code that solves the Vlasov-Maxwell system in one spatial and momentum dimension. Adaptive mesh refinement may be one way to limit the unfavourable scaling of the computational cost with the dimension of the problem for continuum methods compared to in the PIC-method. We benchmark the solver and demonstrate speed-ups of the order 7x

compared to if a fixed grid would have been used.

Together with T. C. DuBois, I was responsible for developing and benchmarking the solver for the Vlasov-Maxwell system. I prepared the draft of a major part of the paper, in collaboration with T. C. DuBois, with some additions from E. Siminos regarding semi-analytical solutions in Section 4.1. The paper was finalized in collaboration between the co-authors.

Paper C

Prospects and limitations of wakefield acceleration in solids

In this paper we investigate the effects of using a coherent X-ray pulse to drive wakefield acceleration in solid materials. We verify scalings based on similarity theory, leading to ultra-short electron and photon bunches. Furthermore, we demonstrate that photons are emitted with comparable energies to the accelerated electrons, already at moderate relativistic intensities a_0, making X-ray wakefield accelerators a promising source of high energy photons.

I made the theoretical analysis of the setup, ran the simulations as well as analyzed the results. I prepared the draft, which when was reviewed and finalized in collaboration with my co-authors.

Paper D

Physics of the laser-plasma interface in the relativistic regime of interaction

In this paper we extend the Relativistic Electron Spring (RES) model by relating the γ-factor distribution of electrons to the velocities and layer position in the model. In addition to the RES-parameters, it is shown that the γ-factor distribution is proportional to the layer thickness, which only can be determined by including effects due to the velocity-spread and retardation across the compressed electron sheath.

I made the theoretical derivations in the paper as well as the comparison to simulations. I was responsible for preparing the draft, which was finalized in collaboration with my co-authors.

Contents

Chapter 1

Introduction

Although less present in our immediate surrounding, the plasma state is by far the most commmon state of matter in the universe. In this thesis we consider the interaction of high intensity laser light with plasmas, its numerical modelling, and some of its applications to particle acceleration and radiation generation. The topic has been sparked by the fast development in laser technology since the realisation of the first laser by Maiman in the year 1960 [1]. These advances can to a large extent be attributed to the development of Chirped Pulse Amplification [2] (CPA), which allows to temporally stretch the pulse and hence make it possible to reach high intensities without destroying the laser optics. Contemporary laser systems can reach intensities up to $I \sim 10^{22}\,\mathrm{W/cm^2}$, which is higher than focusing all sun light reaching the face of the earth to an area similar to the tip of a hair. There is today a multitude of high intensity laser facilities [3, 4, 5].

One may ask what is achieved by shining high intensity laser light on matter: First of all, if the intensity is high enough to compete with the Coulomb field binding electrons, matter will be ionized forming a plasma. This already occurs at, by todays standards, modest intensities of $I \sim 10^{16}\,\mathrm{W/cm^2}$. Contemporary laser pulses have μm wavelength and spatio-temporal extension of a few wavelengths meaning that they can probe very short space- and time-scales. By increasing the intensity further, particles can be accelerated to relativistic energies within one laser cycle, i.e. gain a speed close to the speed of light. The threshold for the onset of relativistic motion of a particle can be estimated by $I \approx 2.8 \cdot 10^{18}(m/m_e\lambda)^2$, where λ is the wavelength in μm and m/m_e is the particle mass relative to the electron mass.

For electrons and an optical wavelength laser, the threshold becomes $I \sim 10^{18}\,\mathrm{W/cm^2}$. Upon entering the regime of relativistic intensities, the electron dynamics becomes strongly nonlinear. This both allows for a multitude of schemes for particle acceleration as well as conversion of the laser frequency into higher frequencies of radiation [6, 7, 8]. However, ions, which are much heavier than electrons, respond more slowly and still gain velocities significantly below the speed of light. By further increasing the intensity to $I \sim 10^{24}\,\mathrm{W/cm^2}$, light ions reach relativistic velocities. The onset of significant ion mobility drastically changes the character of the interaction as ions start to respond to the fields at a timescale similar to that for electrons. As laser intensities increase further, effects such as radiation losses become significant, which, depending on the intensity and wavelength regime, can be described by classical models or need a full quantum treatment, incorporating the stochasticity of photon emission. The prescence of radiation reaction has been demonstrated in recent experiments [9, 10]. In the parameter regime of strong radiation reaction (either classical or quantum), the dynamics of electrons no longer follows the paths implied by the Lorentz force, but are guided along a so called radiation free direction [11]. For higher intensities, approaching the Schwinger-limit, there are further possibilities to study the quantum nature of matter, involving non-perturbative pair-creation as well as other higher order processes.

As laser plasma interaction is strongly nonlinear, numerical methods are necessary to assist the understanding from analytical models and in detail describe the properties of the interaction. However, adapting a single-particle picture and numerically accounting for the paths of all particles is well beyond the capabilities of existing and foreseeable computing resources. Instead, all computational models need to resort to some sort of approximation, for example as in kinetic or fluid models. Kinetic models are necessary for problems where the velocity distribution of the plasma particles is essential, which often is the case. The Particle-In-Cell (PIC) method [12, 13] is nowadays a standard tool for kinetic modelling of laser plasma interaction. In this method, the single particles are sampled and a limited number of macro-particles are tracked, whose paths are calculated, with the electromagnetic fields self-consistently advanced on a grid for the spatial dimensions. The PIC-method has also been successful to incorporate QED effects, as the stochastic event of emission of a photon or creation of an electron-positron pair relies on that the particle picture to some

extent is maintained. This is of interest for modelling prospective experiments in next generation laser facilities, e.g. the Extreme Light Infrastructure (ELI) [14].

One of the foremost strengths of the PIC-method – that it samples velocity space – is also a shortcoming for a limited range of applications where a detailed noise-free description of velocity space is critical. This is also the case for problems where collisional processes are important. For these problems, continuum methods may need to be used, which discretise the distribution function and solve the Vlasov-Maxwell system of equations on a phase space grid [15]. However, the use of a grid incorporating the velocity dimensions comes at the disadvantage that the problem becomes computationally more demanding. Solvers for the Vlasov-Maxwell system are therefore primarily used when it is possible to consider a model with reduced dimensionality. In this thesis, some attention is paid to the development of efficient Vlasov-Maxwell solvers, e.g. utilising an adaptive grid, to reduce the computational costs.

Applicationwise, the existence of lasers with ultra-high fields in combination with short duration and tight focusing has given rise to a range of possibilities, including particle accelerators [6, 7], inertial confinement fusion [16] and high frequency radiation generation [8]. Practical applications derived from these topics, of great interest to society, also include medical treatment and diagnosis as well as non-destructive testing and imaging [17, 18, 19, 20]. In contrast to conventional particle accelerators such as SLAC [21] and LHC [22] aimed at providing/probing high/extreme energies (GeV and TeV scales), the electric fields achievable in plasma accelerators are to a high degree scalable with the intensity of the laser light, whereas in the former case, there are more restricting limits of the order 10-100 MV/m due to the breakdown of semiconductors. In contemporary laser-plasma experiments, gradients of the order 100 GV/m have been reached [23] making laser-plasma accelerators a candidate for achieving more compact particle accelerators, which will be of benefit in the quest for even higher particle energies.

For electron acceleration, lasers can be used to drive plasma waves moving with velocities close to the speed of light, trapping and accelerating electrons [24]. This is known as wakefield acceleration and has been demonstrated to provide high quality scalable electron beams of several GeV [23]. Whereas contemporary wakefields are driven by

optical wavelength lasers (or particle beams), in this thesis, we treat the effects of using an X-ray pulse to drive the wake. The possibility of laser-plasma generated relativistically intense X-ray pulses that could be used for such experiment has previously been demonstrated in simulations [25]. When reducing the wavelength, both the importance and character of QED-effects increases/changes compared to at optical wavelength.

For ion acceleration, and laser intensties below the threshold for relativistic ion motion, the high mass of ions prevents trapping in moving structures with velocities close to the speed of light and different approaches must be adopted. The laser field needs to be converted into a slow-moving field structure to allow for acceleration. With the first mentioning of plasma based ion accelerators in 1957 by Veksler [26], several laser-plasma based techniques for ion acceleration have today been devised. Target Normal Sheet Acceleration (TNSA) is one of the most studied schemes [7, 27]. Whereas TNSA is very robust and can have a high conversion efficiency of laser energy into energy of the plasma particles, the acceleration process leads to ions with a thermal spectrum. Other methods, for example shock acceleration where ions are reflected by a moving potential barrier can provide a monoenergetic spectrum, which is beneficial for applications. However, the conversion of laser energy into ion energy is less efficient and obtaining a significant number of accelerated particles is challenging. Continuum methods are beneficial for modelling shocks, which therefore are considered in connection to the continuum solvers that are implemented as a part of this work.

Acceleration of charged particles moving at relativistic speeds provides the foundation for several schemes for the generation of short frequency radiation, for example in the X-ray regime. In conventional particle accelerators, short wavelength synchrotron radiation can be created from the bending of the particle path in an accelerator ring. Whereas the radiation presents an energy loss mechanism for the accelerated particles, which may be undesired if high energies are sought such as at the LHC, X-ray sources are of great importance to a range of applications, for example condensed matter physics, material science, biology and medicine. Other types of X-ray sources include the Free-Electron-Laser (FEL) [28], which also derives from the concept of synchrotron radiation, but with an electron beam wiggling along a straight path through an alternating field. Different sources are asso-

ciated with different properties and possibilities. Laser-plasma based sources of coherent X-ray pulses [29, 30, 31] make use of the non-linearity of the equations of plasma physics to convert the frequency of the laser radiation into a signal with high frequency content, with prospects of producing high brilliance, high intensity coherent X-ray pulses. This thesis approaches scalings with the intensity of the laser for properties such as the frequency range and amplitude of attosecond pulses generated from the interaction.

Outline

This thesis is organised as follows: In Chapter 2, we define the plasma state and formulate the governing equations, as well as give an overview of some additions from QED that must be considered at high intensities. This is followed by Chapter 3, which reviews basic waves in plasma, the electron motion in a plane-wave laser field and the effect of pulse shape manifest through the ponderomotive force to give a flavour of the properties of plasma dynamics. Furthermore, some aspects of electron wakefield acceleration and shock driven ion acceleration are treated, which are the topics of Papers A and C. In Chapter 4, the PIC-method is discussed, as well as compared with continuum methods for the Vlasov-Maxwell system of equations, connecting to Papers A and B. Chapter 5 then reviews topics concerning radiation generation from laser-plasma interaction, as well as elaborates on the spectrum for electrons at the vacuum-plasma interface and its micro-dynamics, which relates to Paper D. Finally, Chapter 6 gives an overview of the papers that are included in this thesis, as well as the contribution by the author.

Chapter 2

The equations of plasma physics

A plasma is defined as a quasi-neutral ionized gas which exhibits collective behaviour, i.e. a state which consists of freely moving charges: electrons, ions and potentially positrons, that interact through long range electromagnetic fields. This is different from ordinary matter, such as solids, liquids and gases, where short range interactions between nearest neighbours play a more important role. A more quantitative understanding of the definition of a plasma can be obtained by considering the effect of a small test charge, with charge q, in a plasma with background density n_0. The plasma then sets up a density perturbation and potential ϕ described by

$$n_e = n_0 \exp(e\phi/k_B T_e) \quad \text{and} \quad \phi = \frac{q}{r} \exp(-r/\lambda_D)$$

where r is the distance to the particle, k_B is the Boltzmann constant, T_e the temperature of the electrons, e the elementary charge and λ_D is the Debye length [32], defined by

$$\lambda_D = \sqrt{\frac{k_B T_e}{4\pi n_0 e^2}}.$$

The potential should be compared to the Coulomb potential of the particle: q/r. It is clear that the plasma acts to shield the effects of individual charges with a characteristic scale of λ_D. This model breaks down if λ_D is too small compared to the average particle distance. The conditions for quasi-neutrality and dominance of collective effects can

hence be expressed in terms of $n_0\lambda_D^3 \gg 1$, i.e. that a volume with dimensions of the Debye length must contain many particles.

In the field of laser plasma interaction, a laser pulse is commonly incident on a plasma-vacuum surface. The character of the dynamics depends on a number of factors, e.g. the amplitude, shape and duration of the pulse, as well as the plasma profile and density. Laser pulses can commonly be approximated by

$$\vec{E}(x,y,z,t) = E_y(x-t/c,y,z)\sin(\omega t-kx)\hat{y}+E_z(x-t/c,y,z)\sin(\omega t-kx+\psi_0)\hat{z}$$

where the x-axis is assumed to be aligned with the axis of incidence of the pulse and E_y, E_z are assumed to vary slowly compared to the temporal and spatial scales implied by ω^{-1} and k^{-1}. The relativistic amplitude of a laser pulse defined by $a_0 = eE_{\max}/m_e c\omega$, where c is the speed of light, m_e is the electron mass, ω is the angular frequency of the laser and $E_{\max}$ is the maximum electromagnetic field strength, is an important scale for the degree of relativistic motion in the interaction. It defines a typical energy scale: $\epsilon = m_e c^2(\gamma - 1) \approx a_0 m_e c^2$ (γ is the gamma factor) for electrons interacting with the laser field. In Section 3.2, the relativistic amplitude is connected to the electron motion for electrons interacting with a plane wave; for which analytical solutions exist and are well known.

To describe the plasma dynamics, it is necessary to self-consistently account for the dynamics of all plasma particles and the electromagnetic fields [33]. This can, for a classical plasma, be done by solving the equations of motion of the particles

$$\begin{aligned}\frac{\mathrm{d}\vec{r}_i(t)}{\mathrm{d}t} &= \vec{v}_i(t)\\ \frac{\mathrm{d}\vec{p}_i(t)}{\mathrm{d}t} &= q_e(\vec{E} + \vec{v}_i(t)\times\vec{B}/c),\end{aligned}$$

where $\vec{r}_i(t)$, $\vec{p}_i(t)$ denotes the position and momentum vectors of particle i, $\vec{v}_i(t) = \vec{p}_i(t)/(\gamma m_s)$ is its velocity and m_s, q_s are its mass as well as charge.

$$\vec{F}_L = q_s(\vec{E} + \vec{v}_i(t)\times\vec{B}/c)$$

is the Lorentz force. $\vec{E}$ and $\vec{B}$ are the electromagnetic fields satisfying

Maxwells equations [34], defined by

$$\begin{aligned}\nabla \cdot \vec{E} &= 4\pi\rho \\ \nabla \times \vec{E} &= -\frac{1}{c}\frac{\partial \vec{B}}{\partial t} \\ \nabla \cdot \vec{B} &= 0 \\ \nabla \times \vec{B} &= \frac{4\pi}{c}\vec{J} + \frac{1}{c}\frac{\partial \vec{E}}{\partial t}.\end{aligned}$$

Here, $\vec{J}$ and ρ is the current and charge density, respectively.

Although the many degrees of freedom in the single-particle description provides a full picture, it does in most situations become too complicated to be used to gain substantial insights in the dynamics of the plasma. A more coarse grained description of the plasma dynamics is obtained by noticing that the large number of particles allows for the use of statistical methods, introducing a distribution function $f_s(\vec{x},\vec{p},t)$, where s is an index for the species and $\vec{x}$, $\vec{p}$ are position and momentum coordinates for a six dimensional phase space. This distribution function describes the number of particles $dN = f_s(\vec{x},\vec{p},t)\mathrm{d}^3\vec{x}\mathrm{d}^3\vec{p}$ in a phase-space volume $\mathrm{d}^3\vec{x}\mathrm{d}^3\vec{p}$. For collisionless plasma, the distribution function satisfies a continuity equation known as the Vlasov-equation [35, 36]

$$\frac{\partial f_s}{\partial t} + \frac{p_i}{m_s\gamma_s}\frac{\partial f}{\partial x_i} + q_s\left[E_i + \frac{1}{\gamma_s m_s c}(\vec{p}\times\vec{B})_i\right]\frac{\partial f}{\partial p_i} = 0$$

with $\gamma_s = \sqrt{p^2/m_s^2c^2 + 1}$. Using the distribution function, the charge and current densities can be expressed as

$$\vec{J} = \sum_s \frac{q_s}{m_s}\int \frac{\vec{p}}{\gamma_s} f_s \,\mathrm{d}^3p$$

and

$$\rho = \sum_s q_s \int f_s \,\mathrm{d}^3p,$$

where the summation ranges over all species s in the plasma.

In the derivation of the Vlasov-equation, the transition from the particle description to the distribution $f_s(\vec{x},\vec{p},t)$ is performed through an averaging process. As a consequence, detailed information about the field structure is transferred into a collision term. The collision

term has contributions from the interactions between the individual particles, typically modelled as binary interactions. Because of the short time scale of a collisional event, it can be modelled by a cross-section leading to a disruptive change of the particle momenta. In fusion plasmas, collisional processes are of paramount importance. However, in laser-plasma physics, the typical time scale of plasma dynamics is defined by the laser period and is short compared to the average time between collisional events. This can be indicated by estimating the (electron-ion) collision frequency for relativistic electrons: $v_{ei} = 4\pi n_e Z c r_0^2 \log\Lambda/\gamma^2$, where Z is the charge number for ions, $\log\Lambda$ is the Coulomb logarithm and r_0 is the classical electron radius. Taking typical values $\log\Lambda \sim 10$, $Z \sim 10$ and $\gamma \sim a_0$, assuming $a_0 \sim 10$ for contemporary laser facilities, the collision frequency is $v_{ei} = 3 \cdot 10^{-18} n_e$. Typical densities for plasmas range from $n_e = 10^{18}\,\mathrm{cm}^{-3}$ to $10^{24}\,\mathrm{cm}^{-3}$ for gas jets and solids respectively. Consequently v_{ei} ranges between 3 Hz to 3 MHz, which can be compared to the laser frequency $f = 300\,\mathrm{THz}$ for optical wavelengths ($\lambda = 1\,\mu\mathrm{m}$). Furthermore, as the collision frequency decreases with the electron energy, collisional effects are less important for particle beams reaching high energies, e.g. electron beams in wakefield acceleration.

In Papers A and B, we consider a Vlasov-equation of reduced dimensionality, with only one spatial (x) and momentum (p_x) direction respectively. For a problem where the transverse variations in the laser and plasma density (with respect to the propagation direction x) are small, the Hamiltonian for a plasma particle is

$$H = m_s c^2 \left[1 + \frac{(\vec{\Pi}_s - q_s \vec{A}/c)^2}{m_s^2 c^2} \right]^{1/2} + q_s \phi$$

and only depends on x. Here, ϕ is the electrostatic potential and $\vec{A}$ is the vector potential, defined by $\vec{E} = -\nabla\phi - c^{-1}\partial\vec{A}/\partial t$ and $\vec{B} = \nabla \times \vec{A}$, respectively. This yields conservation relations for the transverse canonical momentum: $\Pi_{s\perp} = q_s A_\perp/c + p_\perp = 0$, which can be used to reduce the Vlasov-equation to one dimension. One dimensional models are also applicable in cases where a laser impinges on a surface at an oblique angle (by using a Lorentz transformation).

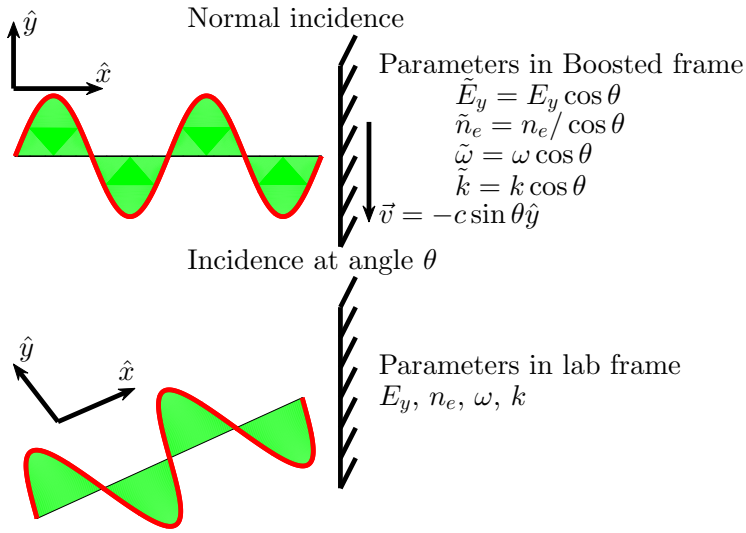

Figure 2.1: For a plane wave E_y incoming at an angle θ with respect to a plasma surface, a Lorentz transformation by the velocity $c \sin\theta$ along the plasma surface converts the problem into that of normal incidence, after transforming the fields and plasma density as indicated in the Figure. As a result of the Lorentz transformation, the electrons and ions have an initial velocity of $\vec{v} = -c \sin\theta \hat{y}$ in the boosted frame.

2.1 Oblique to normal incidence

From special relativity it is known that the laws of physics are the same in all inertial frames and that the coordinates in these frames transform in such a way that the Minkowski metric is invariant [37]. When studying the interaction of lasers and plasma, we are therefore free to choose a reference frame which makes calculations as convenient as possible and may then relate quantities in this frame through a Lorentz-transformation to quantities that may be measured in the lab frame. In the majority of experiments the laser is impinging at an angle θ with respect to the surface normal of the plasma, whereas normal incidence is less common as reflection of laser light would damage the optics of the laser. However, it is analytically (as well as numerically)

challenging to solve the equations of laser-plasma interaction in two or more spatial dimensions. In this situation, a Lorentz transformation can be used, associated with the velocity $c\sin\theta$ along the surface of the plasma, as shown in Figure 2.1, to transform the two-dimensional physics associated with oblique incidence to that of normal incidence in one dimension (provided that the incoming laser has infinite transverse width) [38]. By the definition of the Lorentz transformation, the physical laws in the new frame are the same as in the original one, although properties such as space, time, field strengths and densities are transformed. In this particular case, quantities in the lab frame transform according to the following

$$\begin{aligned} k &\to k\cos\theta \\ \omega &\to \omega\cos\theta \\ E_y &\to E_y\cos\theta \\ n_e &\to n_e/\cos\theta \end{aligned}$$

where k is the wave-vector of the laser radiation, ω is the angular frequency, E_y is the transverse electrical field in the plane of incidence and n_e is the plasma density in the lab frame. In the boosted frame, electrons and ions have an initial velocity of $\vec{v} = -c\sin\theta\hat{y}$, leading to that unshielded ions generate a magnetic field. This transformation is for example useful to describe the dynamics of the laser-plasma interface and high-harmonic generation from laser plasma interaction at an arbitrary angle of incidence [31], which is of relevance to Chapter 5. On the other hand, although the Lorentz transformation is generally valid, it only results in a problem of lower dimensionality if the laser has a constant transverse amplitude. If the laser has a spot-size that is comparable to the transverse amplitude of oscillation of electrons, the transformed problem may be equally challenging as the original one at oblique incidence.

Another area of laser-plasma physics which benefits from Lorentz transformation is electron wakefield acceleration. In wakefield acceleration, which is presented in Chapter 4, a moving cavity is formed, which travels at a speed close to the speed of light; accelerating electrons to high energies while traversing long distances compared to the scale of the cavity. In this case, a Lorentz-transformation to a frame co-moving with the cavity can significantly reduce the computational demands compared to resolving the entire traversed distance.

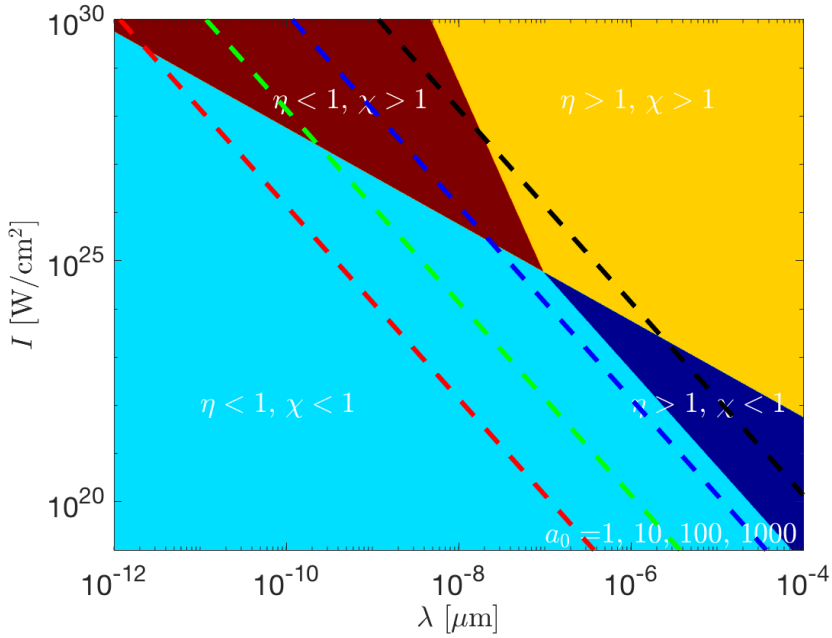

Figure 2.2: The wavelength and intensity for a laser pulse can result in different regimes of interaction with respect to radiation reaction: A regime with small quantum parameter χ and low emission frequency η (light blue), a region with small χ and moderate to high η (dark blue), a region with high χ and low η (dark red) as well as a region with both high χ and η (yellow). Notice the lines indicating relativistic intensity a_0 =1 (red), 10 (green), 100 (blue) and 1000 (black).

2.2 Radiation reaction and QED-effects

In the classical picture, electromagnetic waves are radiated from accelerated charges. In contrast to this description in terms of fields, quantum electrodynamics (QED) dictates that light is mediated by particles, more precisely photons, and that radiation can be interpreted as the emission of these particles. The description in terms of photons is necessary to capture the incoherent radiation from high energy particles. The energy of an emitted photon: $E = \hbar\omega_r$, where $\hbar$ is the Planck constant and ω_r is the angular frequency of the photon, equals the energy lost by the radiating particle. The dominant contribution comes from synchrotron radiation, which is due to acceleration transverse to

the particle velocity. For relativistic particles, synchrotron radiation results in photon emission with a typical frequency

$$\omega_r = \frac{3}{2}\omega_0\gamma^3$$

where ω_0 is the non-relativistic synchrotron frequency. Hence; particles with small mass, which can gain large relativistic factors γ by interacting with the laser field, i.e. electrons and potentially also positrons, are responsible for radiation of high energy photons. It is evident that the energy of the emitted photons grows quickly with the intensity of the laser ($\omega_r \sim a_0^3$) and can for relativistically intense laser pulses be significantly higher than the frequency of the laser radiation ω.

The character of the radiation is influenced by the value of the dimensionless parameter

$$\chi = \gamma E_\perp / E_c$$

where γ is the gamma-factor of a radiating particle, $E_\perp$ is the transverse electric field experienced by the particle and $E_c = m_e^2c^3/e\hbar$ is the Schwinger field. In the classical regime, for which $\chi \ll 1$, χ is proportional to the ratio between the energy of a typical emitted photon and the energy of the radiating particle: $2\hbar\omega_r/3\gamma m_e c^2$. For $\chi \ll 1$, since the fraction of the particle energy that is lost by emitting one photon is small, the emission of radiation only affects the particle dynamics if emission events are frequent. In that case, the effect on the particle dynamics can be described by a continuous force, e.g. the Landau-Lifschitz force [39], which to leading order takes the form

$$\vec{f} = -\frac{2}{3}\frac{e^2 m_e^2 c}{\hbar^2}\chi^2\vec{v}$$

where $\vec{v}$ is the velocity of the particle.

The classical treatment using a continuous force for the effect of radiation on the emitting particle, known as radiation reaction, is only valid for $\chi \ll 1$. As χ approaches one, the energies of the photons become similar to those of the emitting particles, leading to recoils which significantly alter the paths of the emitting particles. In this case, it is necessary to describe the radiation in terms of probabilities and cross-sections from QED [40]. The probability distribution for an emission event during an infinitesimal time Δt is given by

$$\frac{\mathrm{d}P}{\mathrm{d}\delta} = \left[\Delta t\frac{e^2 m_e c}{\hbar^2}\right]\frac{\sqrt{3}}{2\pi}\frac{\chi}{\gamma}\frac{1-\delta}{\delta}\left\{F_1(z_q) + \frac{3}{2}\delta\chi z_q F_2(z_q)\right\}$$

where δ is the photon to electron energy quotient, $z_q = 2\delta/3\chi(1-\delta)$ and $F_1(x)$, $F_2(x)$ are the first and second synchrotron functions [40]. In terms of the rate of energy loss for electrons, the total radiated power is

$$I_r = \frac{2e^2 m_e^2 c^3}{3\hbar^3}\chi^2$$

for $\chi < 1$ and

$$I_r = 0.37\frac{e^2 m_e^2 c^3}{\hbar^3}\chi^{2/3}$$

for $\chi > 1$, i.e. the growth of the radiated intensity is slower in the high χ regime.

In qualitative terms, the effect of radiation reaction is determined by the typical ratio of the energy of the emitted photons and the emitting particles, as well as the frequency of emission events. When the intensity of the laser increases, both the typical energy fraction and emission frequency is increased. Figure 2.2 divides the parameter space for laser-plasma interaction at different intensities I and wavelengths λ into regions, depending on the corresponding scale for χ and the frequency of radiation events compared with the laser frequency η. Four regions can be identified:

1. A region with $\chi < 1, \eta < 1$ for which radiation reaction is insignificant as emission events are rare and the energies of emitted photons are small compared to those of the electrons.

2. A region $\chi < 1, \eta > 1$, where emission events are frequent but with low energy, resulting in radiation reaction which potentially is significant for the electron dynamics, but which can be described by the classical expressions for the radiation reaction force.

3. A region with $\chi > 1$, $\eta > 1$, where radiation reaction is significant because of large energies of the emitted photons and needs a description from QED. However, the high frequency of emission allows for a treatment in terms of a continuous force.

4. A region with $\chi > 1$, $\eta < 1$ for which emission events lead to significant but stochastic energy losses for the electrons. This region is limited to shorter wavelengths (in the XUV-range).

Using shorter laser-wavelengths in the XUV-regime instead of in the optical regime alters the electron dynamics by allowing the electrons

to enter regions of space with higher field strengths, from which they would be shielded by the more frequent photon emission at optical wavelengths. Hence, letting electrons interact with a relativistically intense laser pulse of nanometer wavelength has been suggested as a method to probe physics at high χ. In Paper C, the effect of using nanometer wavelength pulses to drive wakefield acceleration is investigated. Despite that contemporary high intensity laser sources are operating in the optical regime, generation of short wavelength radiation can be achieved through high harmonic generation. In particular, interaction in the moderately overdense regime allows for the high harmonic signal to maintain a relativistic amplitude of similar order as the incident optical wavelength radiation. One may furthermore notice that as $\chi \sim 1/\lambda$, high χ effects can already be probed at more moderate a_0 if the wavelength is made shorter.

Chapter 3

Some aspects of laser plasma interaction

3.1 Plasma waves and regimes of interaction

The ability of plasma to generate electromagnetic fields and self-organize leads to many different plasma wave modes. A basic example is the so called Langmuir waves. If the density of an otherwise neutral plasma is perturbed, the plasma will oscillate about its non-perturbed state at a frequency:

$$\omega_p = \sqrt{\frac{4\pi n_e e^2}{m_e}},$$

which is known as the plasma frequency. If the electrons have a finite temperature T_e, the dispersion relation is modified: $\omega^2 = \omega_p^2 + 3k^2(k_B T_e/m_e)$, where k is the magnitude of the wave-vector of the perturbation.

Electromagnetic waves are a different kind of waves, describing the propagation of electromagnetic fields in the presence of a plasma. Their dispersion relation is:

$$\omega^2 = \omega_p^2 + k^2 c^2$$

which in the limit of $\omega_p = 0$ (i.e. the plasma density is zero) coincides with the ordinary dispersion relation for light in vacuum.

Notice that the dispersion relation for electromagnetic waves has a lower frequency threshold ω_p. It is consequently only possible for electromagnetic waves to propagate if their frequency ω is higher than the plasma frequency ω_p. Conversely, there is a critical (maximum)

plasma density for which an electromagnetic wave with frequency ω can propagate in the plasma:

$$n_c = \frac{\omega^2 m_e}{4\pi e^2}.$$

If the laser pulse is strong enough to accelerate the electrons to relativistic energies, this threshold is modified by relativistic effects by replacing the electron mass with its relativistic counterpart $m_e\gamma$. Furthermore, this result applies for propagation of a wave that already is inside the plasma. If a laser pulse impinges on a vacuum plasma interface, the electrons reorganize themselves and the threshold for propagation is different. This will be discussed in Section 3.4. The threshold can be interpreted as the critical level of the density such that the current generated by electrons within the skin depth is large enough to counteract the incoming field.

The existence of a threshold density for propagation of light divides laser plasma interaction in two distinct regimes: An underdense regime where the density is below the threshold, hence allowing propagation of laser pulses, as well as an overdense regime in which the laser light is reflected and/or absorbed at the vacuum plasma interface. The waves excited by the laser pulse in the underdense regime move at a speed close to the speed of light, and this regime is therefore commonly used for electron acceleration. On the other hand, ions are more than a thousand times heavier than electrons and therefore respond more slowly to electromagnetic fields. This results in that they are not as efficiently accelerated by fast-moving plasma waves. Instead, ion acceleration often utilizes quasi-stationary fields which can be set up by interaction in the overdense regime.

3.2 Single particle dynamics

Basic understanding of the interaction of laser light and plasma can also be gained by considering the interaction of a single electron with an incoming electromagnetic field. For example, consider the interaction of an electron with a linearly polarized wave, described by the vector potential $\vec{A} = A_y(\psi)\,\hat{y}$, where $\psi = kx - \omega t$ is a phase coordinate. In

this case, the evolution of particle momenta obeys

$$\frac{\mathrm{d}p_x(t)}{\mathrm{d}t} = \frac{e\omega}{c}\frac{\partial A_y(\psi)}{\partial\psi}\frac{v_y}{c},$$
$$\frac{\mathrm{d}p_y(t)}{\mathrm{d}t} = \frac{e\omega}{c}\frac{\partial A_y(\psi)}{\partial\psi}\left(1-\frac{v_x}{c}\right).$$

Furthermore, the change of energy of the electron can be written as

$$\frac{\mathrm{d}\gamma}{\mathrm{d}t} = \frac{e}{m_e c^2}\vec{v}\cdot\vec{E} = \frac{e\omega}{m_e c^2}\frac{\partial A_y(\psi)}{\partial\psi}\frac{v_y}{c}.$$

In addition to the constant of motion arising from the conservation of canonical momentum, $\Pi_y = eA_y/c + p_y$, combining the equations for evolution of p_x and γ provides the constant

$$\Gamma = \gamma - \frac{p_x}{m_e c}.$$

The evolution of the phase of an electron interacting with the laser field can hence be written as

$$\frac{\mathrm{d}\psi}{\mathrm{d}t} = -\frac{\Gamma\omega}{\gamma},$$

which shows that the electron is increasingly locked in phase as its energy increases. Lets further assume that the electron, initially positioned $x = y = 0$ at $t = 0$, is at rest, i.e. $\Pi_y = 0$ and $\Gamma = 1$, as well as that the incoming laser field can be described by $A_y(\psi) = A_0 \sin\psi$. In that case

$$kx = -\frac{a_0^2}{4}\left(\psi - \frac{1}{2}\sin 2\psi\right)$$
$$ky = a_0(1-\cos\psi)$$
$$\gamma = 1 + \frac{a_0^2}{2}\sin^2\psi$$
$$\omega t = -\psi - \frac{a_0^2}{4}\left(\psi - \frac{1}{2}\sin 2\psi\right).$$

For this motion, the average drift-velocity

$$v_d = \frac{a_0^2 c}{4 + a_0^2}$$

defines an average rest frame, and after making a Lorentz transformation corresponding to this velocity, the motion becomes

$$k\tilde{x} = \frac{a_0^2}{8(1+a_0^2/2)^{1/2}} \sin 2\psi \quad \text{and} \quad k\tilde{y} = a_0(1-\cos\psi)$$

which describes an electron moving in a path similar to a figure-eight.

From the solution for the motion of an electron in a plane wave one may notice that the electron mostly oscillates orthogonally to the axis of the incoming electric field for non-relativistic field amplitudes ($a_0 < 1$). On the other hand; for relativistic amplitudes, the forward drift velocity increases towards the speed of light and the motion becomes more directed forward. However, the γ-factor oscillates with the phase in the laser field and the electron does consequently not gain any energy from the interaction with an even number of laser periods [41]. To achieve a net acceleration, one may instead modify the fields [42] by the presence of a plasma, boundary or by focusing of the laser pulse. In this case a net acceleration can occur as the electron traverses regions of different intensity, also known as ponderomotive acceleration. Furthermore, in the particular case of tight focusing; the small transverse dimensions of the pulse can give rise to substantial electric fields in the propagation direction; resulting in phase locking and consequent acceleration to high energies, known as direct laser acceleration [43].

3.3 The ponderomotive force

The situation of an electron interacting with an inhomogeneous laser field is conceptually different from that of interaction with a plane wave with constant amplitude, for which the displacement of the electron does not affect the amplitude of the experienced field. In this case, the variation of the envelope amplitude across the fast time scale of oscillation of the electron acts as a force expelling particles from regions with strong fields. This is most easily derived in the regime of weak fields, which will be done here, but with generalizations to the regime with relativistic dynamics [44]. In this case, consider an electro-magnetic field defined by

$$\vec{E}(\vec{r},t) = \vec{E}(\vec{r})\cos\omega t$$
$$\vec{B}(\vec{r},t) = -\frac{c}{\omega}\nabla \times \vec{E}(\vec{r})\sin\omega t$$

where the magnetic field has been related to the electric field through Faradays law $c^{-1}\partial\vec{B}/\partial t = \nabla \times \vec{E}$. An equation of motion can then be written as

$$m_e \frac{\mathrm{d}\vec{v}}{\mathrm{d}t} = e\left(\vec{E}(\vec{r})\cos\omega t - \frac{\vec{v}}{\omega} \times \left[\nabla \times \vec{E}(\vec{r})\right]\sin\omega t\right).$$

Now, lets decompose the motion into a fast ($\vec{r}_f$) and slowly ($\vec{r}_s$) varying part such that $\vec{r} = \vec{r}_s + \vec{r}_f$, where $\vec{r}_s$ can be interepreted as a cycle-averaged motion. By solving for the fast motion, given by

$$\vec{r}_f = -\frac{e\vec{E}(\vec{r}_s)}{m_e\omega^2}\cos\omega t \quad \text{and} \quad \vec{v}_f = \frac{e\vec{E}(\vec{r}_s)}{m_e\omega}\sin\omega t$$

it is then possible to write down an equation for the cycle-averaged motion $\vec{r}_s$:

$$m_e \frac{\mathrm{d}\vec{v}_s}{\mathrm{d}t} = -\frac{e^2}{2m_e\omega^2}\left((\vec{E}(\vec{r}_s)\cdot\nabla)\vec{E}(\vec{r}_s) + \vec{E}(\vec{r}_s)\times(\nabla\times\vec{E}(\vec{r}_s))\right)$$

which can be rewritten as

$$m_e \frac{\mathrm{d}\vec{v}_s}{\mathrm{d}t} = -\nabla\Phi$$

where

$$\Phi = \frac{e^2}{4m_e\omega^2}||\vec{E}(\vec{r}_s)||^2$$

acts as a ponderomotive potential, expelling particles in the direction of decreasing fields.

3.4 The effect of vacuum plasma interface

For a stationary circularly polarized laser pulse incident on a vacuum plasma interface of a one-dimensional step-like overdense cold plasma, semi-analytical solutions exist for the stationary state reached by the plasma [45, 46, 47]. In Papers A and B, such solutions have been used to verify the correctness of implemented solvers for the Vlasov-Maxwell system. Under these circumstances, the cold fluid equations can be used. Assuming that $p_x = 0$ at an equilibrium, the cold fluid equations can be written in the form

$$\frac{\mathrm{d}\phi}{\mathrm{d}x} = \frac{\mathrm{d}\gamma}{\mathrm{d}x},$$

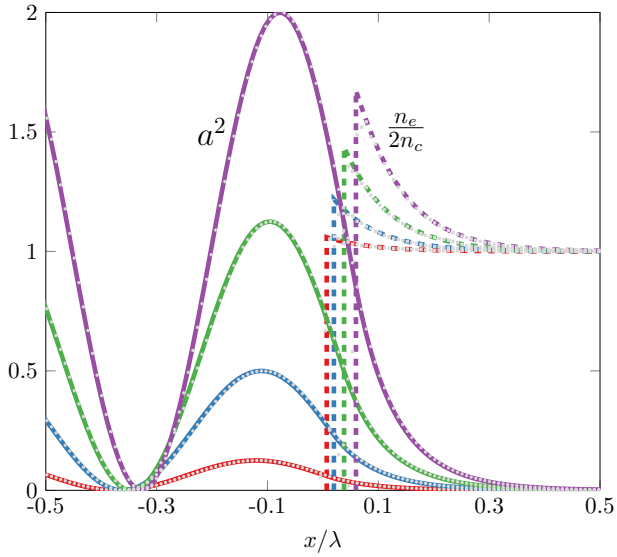

Figure 3.1: Plasma densities and vector potential for stationary solutions when a circularly polarized laser pulse impinges on a step-like plasma of initial density $2n_c$. The densities have been normalized by $2n_c$, to fit on the same scale as the squared vector potential. The analytical results for different intensities are labelled with the colours red ($a_0 = 0.25$), blue ($a_0 = 0.50$), green ($a_0 = 0.75$) and purple ($a_0 = 1.00$). Numerical results are coloured in grey.

$$\frac{\mathrm{d}^2\phi}{\mathrm{d}x^2} = n_e - n_0,$$
$$\frac{\mathrm{d}^2 a}{\mathrm{d}x^2} = \left(\frac{n_e}{\gamma} - 1\right) a,$$

where n_0 is the unperturbed plasma density, n_e is the electron density resulting from the interaction with the laser pulse, ϕ is a normalized electrostatic potential, a is the vector potential and $\gamma = \sqrt{1 + a^2}$. Distance is expressed in terms of wavenumber and field strength in terms of the relativistic electric field $E_r = m_e c\omega/e$.

For a circularly polarized pulse with amplitude a_0, the vacuum plasma surface is pushed by the ponderomotive force leading to a pile up of electrons within a skin depth of the displaced vacuum plasma surface. In the analytical theory, the surface is pushed up to a point x_b at which the electrostatic force due to the displaced charge eE_x

is balanced by the ponderomotive force $-m_e c^2 \partial\gamma/\partial x$. Denoting the value of the vector potential at this point by a_b, it holds that

$$\frac{2a_0^2 + a_b^4}{1 + a_b^2} = 2n_0 \left(\sqrt{1 + a_b^2} - 1 \right).$$

The value of a_b can be found from numerical calculation and x_b can then be calculated by

$$x_b = \frac{a_b}{n_0} \sqrt{\frac{2a_0^2 - a_b^2}{1 + a_b^2}}.$$

Based on these values for x_b and a_b, the normalized vector potential in the vacuum and plasma regions becomes

$$a(x) = \sqrt{2} a_0 \sin \left[\arcsin \left(\frac{a_b}{\sqrt{2} a_0} \right) - (x - x_b) \right]$$

and

$$a(x) = \frac{2\sqrt{n_0(n_0 - 1)} \cosh[(x - x_0)/\lambda_s]}{n_0 \cosh[(x - x_0)/\lambda_s] - (n_0 - 1)},$$

respectively, where $\lambda_s = 1/\sqrt{n_0 - 1}$ is the skin depth and x_0 is determined by ensuring the continuity of the vector potential at $x = x_b$. The electron density is finally calculated from $n_e = n_0 + \partial^2\gamma/\partial x^2$.

In Figure 3.1, the stationary analytical solutions as well as numerical solutions for the electron density and vector potential are shown for circularly polarized pulses of several different a_0 impinging on a plasma of density $n_e = 2n_c$ which initially is located at $x > 0$. In the numerical calculations, the solver in Paper B for the Vlasov-Maxwell system of equations was used. The plasma was assumed to initially have a Maxwellian distributions with a temperature $T_e \approx 0$ and the steady state is reached by interaction with a plane-wave with a rise time of four laser periods. For these parameters, the numerical solutions of the Vlasov-Maxwell system and those based on the semi-analytical formulas agree well. However, for higher field strengths a_0, ion motion effects and the finite rise time of the laser pulse may cause additional heating effects which alter the dynamics, especially for densities close to the critical density [48].

3.5 S-parameter similarity

Laser-plasma interaction comprises a vast parameter space. To understand and optimize the physics it is therefore beneficial if a minimal number of parameters can be considered, from which the essential properties can be inferred. Consider a plasma with electron density n_e interacting with a pulse propagating in the x-direction with vector potential of the form $\vec{a}(x,y,z,t) = a(r_\perp/R,(t-x/c)/\tau)\cos(\omega t - kx)\hat{z}$, where $r_\perp$ is the transverse radial coordinate, R is the width of the pulse and τ is its duration. The interaction can be fully described by the four dimensionless parameters kR, $\omega\tau$, n_e/n_c and a_0. For high a_0, the electrons become relativistic, moving at a speed close to the speed of light and the four dimensionless parameters can be reduced by combining n_e/n_c and a_0 into the similarity parameter $S = n_e/a_0 n_c$, resulting in the three similarity parameters: S, kR and $\omega\tau$ [49, 50]. The S parameter can be viewed as a measure of how overdense the plasma is, incorporating relativistic effects.

At a fixed S-number, both the initial condition for the electromagnetic fields and initial number densities are linear in a_0. As Maxwells equations are linear in the fields and charge as well as current densities, S-similarity theory relies on that there is a limit of the Vlasov-equation that depends on S but not a_0. To indicate this, we introduce

$$\vec{E}' = \vec{E}/a_0, \quad \vec{B}' = \vec{B}/a_0, \quad \vec{p}' = \vec{p}/a_0,$$

and define: $f'(\vec{x},\vec{p}',t) = a_0^2 f(\vec{x},\vec{p},t)$. Using such definitions, the Vlasov equation takes the form

$$\frac{\partial f'}{\partial t} + \frac{p_i'}{m\sqrt{a_0^{-2} + (p'/mc)^2}}\frac{\partial f'}{\partial x_i} + q\left[E_i' + \frac{1}{mc\sqrt{a_0^{-2} + (p'/mc)^2}}(\vec{p}' \times \vec{B}')_i\right]\frac{\partial f'}{\partial p_i'} = 0$$

where the dependency on a_0 is manifest through its appearance in $\vec{v}/c = \frac{\vec{p}'}{mc\sqrt{a_0^{-2}+(p'/mc)^2}}$. The reduction of n_e/n_c and a_0 into the similarity parameter S relies on that the velocity $\vec{v}$ can be approximated by $\vec{v}/c \approx \vec{p}/|\vec{p}|$, which holds if $a_0^{-1} < p'/mc$, where m is the particle mass. S-similarity scaling is for example applicable for wakefield acceleration of electrons in the bubble regime. Another example is the

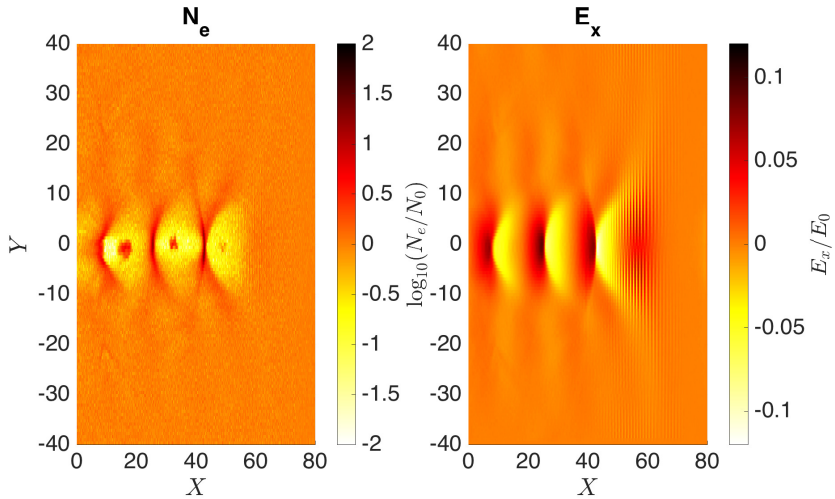

Figure 3.2: Electron density (left) and longitudinal electric field structure (right) for a wakefield in the bubble regime.

dynamics of the position of the vacuum-plasma interface for interaction between a laser and a moderately overdense plasma; as described by the relativistic electron spring model. In this case, the layer dynamics is accurately described by S, without reference to a_0. On the other hand, despite that the high a_0 limit of the Vlasov-equation deceptively indicates that all plasma physics can be described by the S-parameter as long as a_0 is high enough, this turns out to not be the case. For example, in the example of interaction between lasers and moderately overdense plasma, the thickness of the electron sheath that builds up at the vacuum-plasma boundary goes to zero in the limit of high a_0, i.e. the electrons are piled up with infinite density at the vacuum-plasma boundary. The S-similar plasma-dynamics can hence not be used to determine the electron spectrum in the electron sheath, as it is proportional to the thickness, which then also extends to the possibility to determine the spectrum for high harmonics.

3.6 Electron wakefield acceleration

Laser-driven wakefield accelerators were first introduced by Tajima and Dawson [24], almost four decades ago. In an underdense plasma, an

incoming laser pulse propagates at a velocity close to the speed of light and excites a plasma wave co-moving with the pulse. This gives rise to a potential structure moving at a high velocity. If an electron gains a sufficient momentum in the propagation direction of the pulse, it can be trapped in an accelerating phase by the potential structure, and reach high energies. Laser wakefield acceleration has been shown to accelerate electrons to GeV energies [6, 23, 51]. For non-relativistic pulses, defined by $a_0 \ll 1$, the excited wave and density perturbation has a sinusoidal dependence on the phase. If the intensity is increased, reaching a relativistic level $a_0 \sim$ 1-10, which is accessible with contemporary laser systems, nonlinear wake structures where the laser expels all electrons – forming a bubble trailing after the laser pulse – occur. This regime of interaction is known as the bubble regime [49, 52]. Figure 3.2 shows electron densities and the longitudinal electric field for a wakefield in the bubble regime.

3.7 QED-effects in X-ray driven wakefield acceleration

The use of X-ray pulses instead of laser pulses with optical wavelengths to drive accelerating structures (in solid materials) was first suggested by Tajima *et al* in the 1980s [53]. The motivation for this can be derived from the similarity scaling relations which suggest that X-ray driven wakefield acceleration using solid density materials would allow much higher acceleration gradients than if optical wavelengths were used, as well as electron bunches whose temporal and spatial scales have been reduced proportionally to the wavelength. This is interesting for applications demanding extremely short bunches. The electron energies only scale with a_0 and are consequently independent of the wavelength.

In contrast, the radiation from the accelerated electrons in the optical and X-ray driven regime is widely different. The quantum parameter χ scales as $\chi \sim a_0^2(\lambda_c/\lambda)$, where λ_c is the Compton wavelength. A reduction of the wavelength from 1 μm to 5 nm therefore results in an increase of the quantum parameter by a factor of 200. Hence, $\chi \sim 1$ already for $a_0 \sim 50$. In paper C, we investigate the effect of using coherent X-ray pulses to drive wakefield acceleration in the bubble regime, with intensities such that $\chi \sim 1$. This extends the intensity range considered in previous work using PIC-simulations [54, 55] and is mo-

tivated by the theoretical development in generation of high harmonics, specifically the relativistic electron spring model [25, 31, 56, 57], which indicates the possibility to generate nanometer wavelength few cycle X-ray pulses with relativistic intensities.

The effect of the χ enhancement in the X-ray driven regime is to create a wakefield accelerator that emits photons at comparable energies to the electron energies, already at moderate a_0. However, this raises concerns regarding the role of radiation losses and if these will have a deteriorating effect on the accelerating process. Clearly, the discrete nature of photon emission will be crucial for describing the effect of the radiation. The wavelength effects on the radiation emission can be seen by expressing the pre-factor of the emission probability in terms of normalized coordinates: $\chi = \hat{\chi}\, a_0^2(\lambda_c/\lambda)$, $\gamma = a_0\hat{\gamma}$ and $\Delta t = T\Delta\hat{t}$:

$$\frac{\mathrm{d}P}{\mathrm{d}\delta} = \sqrt{3}a_0\,\Delta\hat{t}\,\frac{e^2}{c\hbar}\frac{\hat{\chi}}{\hat{\gamma}}\frac{1-\delta}{\delta}\left\{F_1(z_q) + \frac{3}{2}\delta\chi z_q F_2(z_q)\right\}.$$

It is natural to compare cases of an optical and X-ray driver having the same χ (i.e. different a_0). In that case, the emitted photons have the same spectral shape normalized by the electron energy, but with the emission frequency scaling as $\sim\sqrt{\lambda}$. Using an X-ray pulse to operate a wakefield at a prescribed χ will hence result in fewer emitted photons per electron than at optical wavelengths. On the other hand, if a_0 is kept the same; the higher χ for the X-ray driven case leads to photons with energies closer to those of the electrons.

3.8 Shock acceleration

Paper A treats laser driven shock acceleration of ions. A shock is defined as a propagating structure which changes the macroscopic state over a transition layer. Shock waves can be driven by laser pulses interacting with near critical plasmas: The radiation pressure from the pulse leads to a pile up of electrons on the laser plasma interface, which is pushed to high speed. This leads to the formation of an electrostatic potential structure which continues to travel into the plasma even after the laser pulse has finished interacting with the plasma. The electrostatic structure travels at a velocity v_s (known as the shock-velocity), which in many cases is close to the hole-boring velocity [59, 60]:

$$v_{\mathrm{HB}} = a_0 c\left[(Z/A)(m_e/m_p)(n_c/n_e)(1+R)/2\right]^{1/2},$$

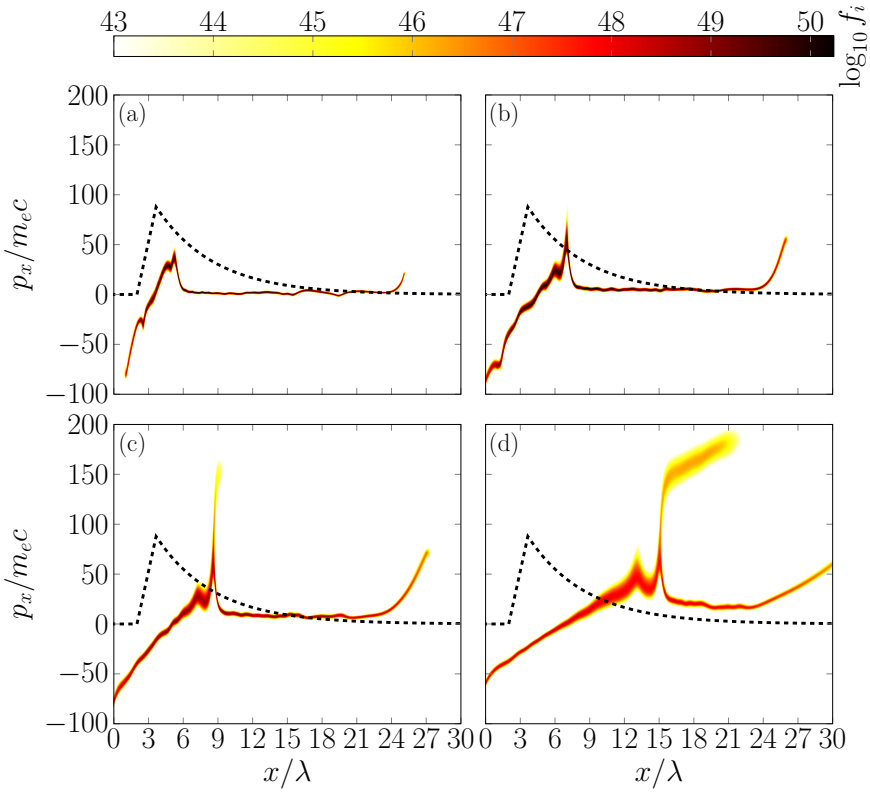

Figure 3.3: Ion distribution function at consecutive instants of time (a to d) for a near critical density plasma interacting with a linearly polarized laser pulse [67]. The initial plasma density has been indicated by black dashed lines.

where Z, A are the charge and mass numbers for the ions and R is the reflectivity of the plasma surface. The symmetry of the up- and down-stream region is broken if the potential is high enough to reflect a fraction of the bulk ions. In the frame of the moving potential structure, the ions are moving at a speed $-v_s$ and are consequently reflected to a speed $2v_s$ in a frame at rest. Provided that the shock only reflects a small fraction of the ions, shock acceleration provides a mono-energetic ion bunch. Figure 3.3 shows a distribution function for ions, with reflected ions, for a shock driven by a linearly polarized laser pulse. Finally, by having a smoothly decaying density down ramp it

is possible to maintain the mono-energetic spectrum of the ions when they exit the plasma [61, 62].

As indicated, the process of laser driven ion shock acceleration contains several steps of energy conversion: First a transfer from the laser to the electrons, followed by part of the electron energy being converted into the electrostatic potential structure moving at the speed v_s. Finally, the energy in the potential structure is converted to ion energy through the reflection process. Efficient realization of shock acceleration therefore builds on optimization of several individual steps, which may be complicated. However, since shock reflection leads to a mono-energetic spectrum, getting enough ions within a specific energy range puts weaker conditions on the conversion efficiency than for methods providing a thermal spectrum. A basic description of ion acceleration using electrostatic shocks is given by Moiseev *et al* [63], which is based on a fluid description for the ions, which takes the reflected ions into account by hand.

In this model, the electron density is assumed to follow a Boltzmann distribution

$$n_e = n_0 \exp(e\phi/k_B T_e)$$

where n_0 is the background density, T_e is the electron temperature and ϕ is the electrostatic potential. The ion (proton) density n_i and velocity v_i satisfy the fluid equations

$$m_i \left(\frac{\partial v_i}{\partial t} + v_i \frac{\partial v_i}{\partial x} \right) = -e \frac{\partial \phi}{\partial x},$$

$$\frac{\partial n_i}{\partial t} + \frac{\partial (n_i v_i)}{\partial x} = 0$$

combined with a Poisson equation

$$-\frac{\partial^2 \phi}{\partial x^2} = 4\pi e (n_i - n_0 \exp(e\phi/k_B T_e))$$

for the potential. It is assumed that all quantities are stationary in a frame moving with the shock velocity, described by the coordinate $\eta = x - v_s t$. These equations can then be transformed into

$$\frac{\partial^2 \phi}{\partial \eta^2} = 4\pi n_0 e \left(\frac{v_s}{\sqrt{v_s^2 - 2e\phi/m_i}} - \exp(e\phi/k_B T_e) \right) \tag{3.1}$$

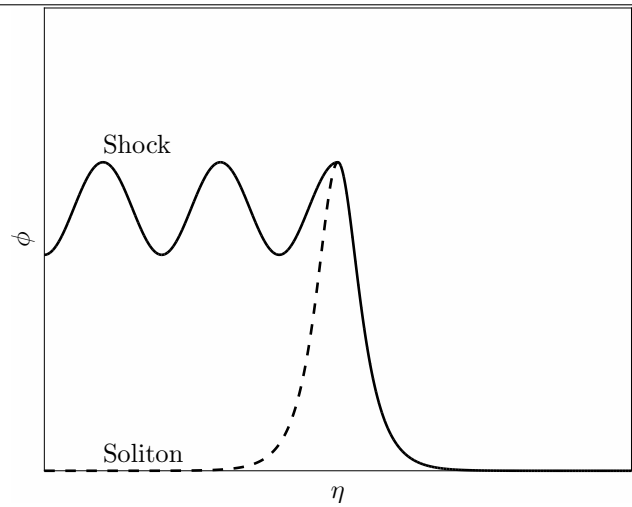

Figure 3.4: Shock and soliton potential structure.

where the right hand side can be expressed as $-\frac{\partial V(\phi)}{\partial \phi}$. $V(\phi)$ is an effective potential taking the form

$$V(\phi) = 4\pi n_0 \left(m_i v_s \sqrt{v_s^2 - 2e\phi/m_i} + k_B T_e \exp(e\phi/k_B T_e) \right).$$

Consequently, the potential satisfies $(\partial_\eta \phi)^2 + V(\phi) = C$ for some constant value C and ϕ can be interpreted as the position of a particle moving in the potential $V(\phi)$, with η taking the role of a time coordinate. Up to this point, the model does not incorporate the effect of reflected ions and is therefore only valid for low enough potential barriers, defined by $\phi \ll v_s^2 m_i/2e$. The solution to (3.1) is symmetric around a maxima of the potential at $\eta = 0$ and the fluid state is left unperturbed after interacting with the potential barrier passing through. This type of solution is known as a solitary wave. For a solitary wave, ions are not accelerated. On the contrary, in a shock wave, the symmetry around $\eta = 0$ is broken by reflection of ions. This occurs when the height of the potential barrier starts to approach $v_s^2 m_i/2e$. The amount of reflected ions for a potential barrier of height ϕ can be quantified by:

$$F(\phi) = \int_{m_i(v_x - v_s)^2/2 < e\phi} f_i(v_x) \mathrm{d}v_x$$

and modifies the Poisson equation in the up- and down-stream regions respectively. This leads to a different potential structure in the up- and down-stream region. Figure 3.4 schematically shows the potential in the soliton and shock case respectively. For steady shock acceleration, the fraction of reflected ions can not be too big as it leads to a quick transfer of the energy in the potential structure to the ions, and consequently a decay of the accelerating field structure. To model shock acceleration it is hence necessary to accurately resolve the low density tail of the ion distribution function. Continuum methods are suitable as they can resolve the low density tail of the ion distribution function with low levels of numerical noise.

As a summary, the benefit of shock acceleration is that the reflection process leads to mono-energetic ions inside the plasma. However, a challenge is how to robustly control the number of ions and achieving a high enough number to be useful for applications, although with promising recent experimental results by Pak *et al* [64]. Other methods for ion acceleration, that also share the property of mono-energetic ion energy spectrum include radiation pressure acceleration [59], light-sail [65] and chirped standing wave acceleration [66], which have different benefits as well as challenges.

Chapter 4

Numerical methods

The Particle-In-Cell method [12] is the most widely used method for kinetic simulations of laser plasma interaction. In this method, the plasma is modelled as an ensemble of particles which is advanced self-consistently with the electromagnetic fields. Consequently, the PIC-method uses a grid for the spatial dimensions of the setup, to represent the fields, but not for the momentum space dimensions of the distribution function. This is efficient as it reduces the size of the computational problem significantly. However, the plasma may still contain a vast number of particles: A solid density material may have a density of $n_e \sim 10^{24}\text{cm}^{-3}$ and a typical length scale of $l \sim 10\,\mu\text{m}$, leading to a total of 10^{15} particles. This is equivalent to 5×10^4 TB of memory in order to store the positions and velocities of the particles, which is well beyond reach for many modern computer systems. The PIC-method does therefore not model the real particles in the plasma, but instead uses super-particles to represent groups of particles which follow the same trajectories by maintaining the same charge to mass ratio as for the real particles.

Figure 4.1 gives an overview of the classical PIC-method. As was touched upon, the classical realization of the PIC-scheme starts from an initial setup of super-particles sampled from an initial distribution function and then consists of a main loop with four steps equivalent to advancing the state by one time step:

1. **Current deposition:** The currents needed for time advancement of the fields are calculated. The super-particles are associated with a shape factor, which describes how the current should be distributed over the grid points. This can allow for higher

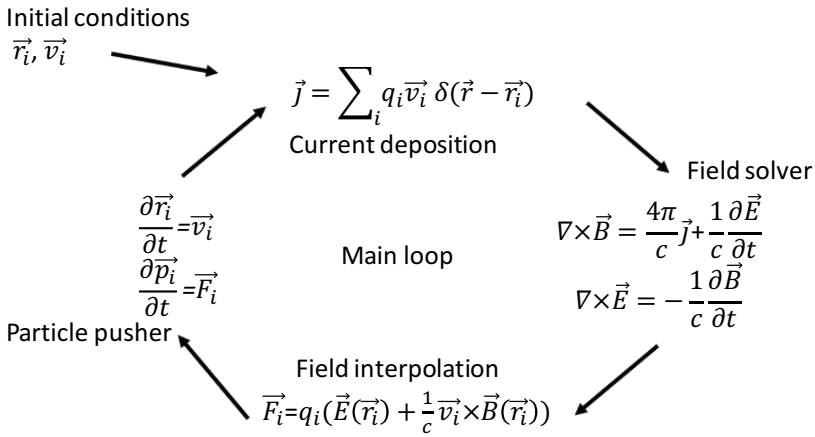

Figure 4.1: Overview of the main loop in the classical PIC-method.

order accuracy compared to if a simplistic view of the particles is adopted.

2. **Field solver:** The field solver advances the electromagnetic fields. There are several different techniques which may be used, for example FDTD (finite difference time domain) [68] and spectral methods. In the former case, the fields are straightforwardly defined on points in real space whereas in the latter case, the fields are represented in Fourier-space and must be transformed to real space when calculating the Lorentz force. Spectral methods are dispersion free and are therefore of great benefit for applications to laser wakefield acceleration, where electrons are co-propagating with a laser pulse at a speed close to the speed of light.

3. **Field interpolation:** Before the particles can be advanced, field interpolation is performed to obtain the electromagnetic fields at the positions of the particles and consequently be able to evaluate the Lorentz force. As in the current deposition, the field

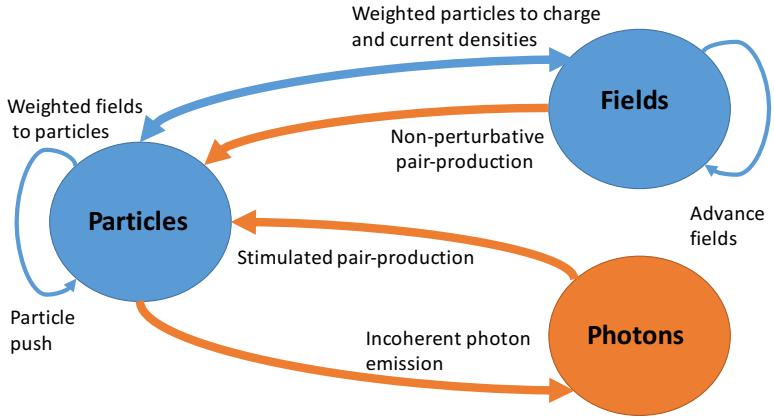

Figure 4.2: The classical PIC-method marked blue, with additions of QED-effects marked orange.

interpolation is performed using a weighting scheme.

4. **Particle pusher:** The equations of motion for the super-particles are integrated. The method which is used to advance the positions of the particles is known as the particle pusher. The Boris-pusher [69] is one of the most common particle pushers, which is a leap-frog method, commonly used because of its excellent long-term accuracy.

The PIC-method renders itself extensible, incorporating new physics, through modules that are executed during different steps of the main loop. This may for example include modules for collisions [70], ionization [71], radiation reaction [72], or, in the strongly relativistic regime, additional QED-effects [40, 73]. QED-effects are for example important in the study of X-ray wakefield acceleration in Paper C. Figure 4.2 indicates the addition of QED-effects to the classical PIC-method [40]. In this case, photons and positrons are added as plasma species, with emission events and pair-creation modelled using statistical routines

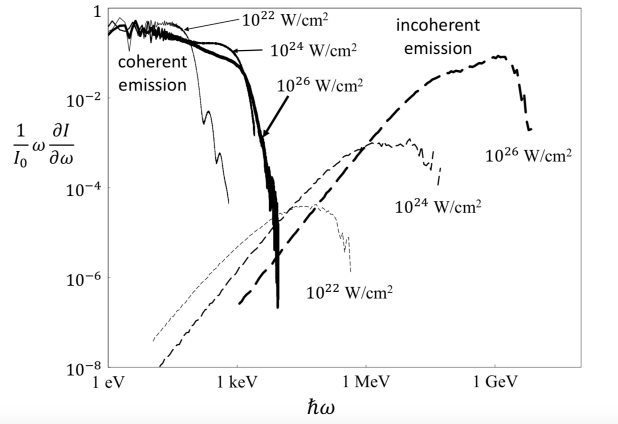

Figure 4.3: Spectra of coherent and incoherent emission. The figure is reprinted from [40].

based on QED-rates. Whereas the addition of positrons is conceptually straightforward, the addition of photons means that there is a dual representation of light: on one hand as the $\vec{E}$, $\vec{B}$ fields and on the other hand as particles. The possibility to split light into these two categories relies on that the radiation spectrum for a particle can be divided into a coherent part with low energy photons, which can be represented as fields, and an incoherent part with high energy photons for which the particle description is necessary. This is illustrated in Figure 4.3, which shows the spectra for coherent and incoherent radiation in a simulation of laser-plasma interaction in the moderately overdense regime. This possibility is an important reason for the success and feasibility of simulations of relativistic laser plasma interaction as the typical frequency for photon emission grows as $\omega_c = 3eH_{\text{eff}}\gamma^2/2m_ec$, where H_{eff} is the effective magnetic field, which otherwise would need to be resolved using a very fine grid already for moderate γ.

4.1 PIC- versus continuum-methods

Continuum methods [74, 75] discretize the distribution function on a grid encompassing both the spatial dimensions and momentum dimensions, i.e. on a grid of dimension $2D$ instead of D as in the PIC-case, where D is the number of spatial dimensions. The PIC-method there-

fore has the advantage of using a smaller grid, which is computationally less costly. Although, the PIC-method is successful for numerical modelling of a majority of problems in laser plasma interaction, it is less suitable when the plasma-dynamics is strongly affected by regions of phase space with low density which only may be assigned a small number of particles. For such problems, the continuum approach to the Vlasov-Maxwell system of equations is more successful.

To estimate which one of the two approaches which is most useful [76] one may first note that in both methods, it is necessary for the spatial grid to resolve the Debye-length λ_D. The number of spatial grid points therefore scales as $N_x^D = (L/\Delta x)^D$ where $\Delta x \sim \lambda_D$ and L is a typical length scale for the problem. The relative performance can be estimated by the number of grid points used by the continuum solver in relation to the number of particles in the PIC-method : $N_{\text{continuum}}/N_{\text{PIC}}$. $N_{\text{continuum}}$ is estimated by $(L/\Delta x)^D N_p^D$, where N_p is a typical number of points to resolve the momentum space dimension. For the PIC-method: $N_{\text{PIC}} = g_p(L/\Delta x)^D$ where g_p is the number of particles per cell. Consequently $N_{\text{continuum}}/N_{\text{PIC}} = g_p^{-1} N_p^D$. For applications where a small number of particles per cell can be used, e.g. laser wakefield acceleration, the PIC-approach clearly has an advantage, whereas continuum methods are more favourable for the study of problems such as shock acceleration [77] or instability growth [78, 76] where a higher number of particles per cell is needed. In summary, continuum methods are preferable if $g_p > N_p^D$, which shows that they are more competitive for low-dimensional systems. Despite being most competitive for $D = 1$, a range of Vlasov-Poisson and Vlasov-Maxwell solvers also exist for $D = 2$ [79, 80] and $D = 3$ [81, 82].

A number of approximations have been made in reaching the comparison in the previous paragraph: Firstly, g_p is affected by factors such as the shape function used in the PIC-code, and the order of accuracy for the method used by the continuum solver also plays a role, both with regard to the number of needed grid points and the computational cost per grid point to take one time step. However, one may still argue that $N_{\text{continuum}}/N_{\text{PIC}}$ gives an indication of the relative competitiveness for different D. On the other hand, if it would be possible to use an adaptive mesh [83] which limited the number of grid points, by only applying high resolution in regions where it is needed, it could be possible to limit the unfavourable scaling for continuum methods with the dimension of the problem. Figure 4.4 shows the representation of

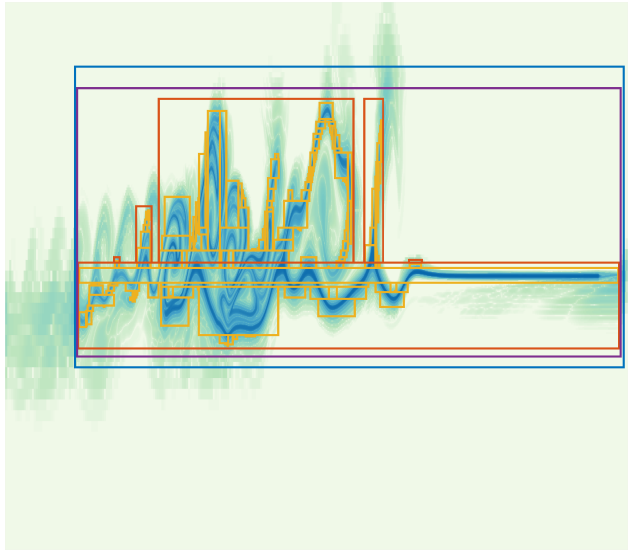

Figure 4.4: Distribution function represented on an adaptive mesh. By only applying high resolution in regions carrying significant information, it is possible to mitigate parts of the additional costs due to the momentum space grid in the continuum approach compared to in the PIC-method.

a distribution function resulting from the interaction of a laser with a plasma using an adaptive grid. The grid consists of five levels of different coarseness, with higher resolution limited to regions that carry significant information. Benefits from the use of an adaptive mesh is treated further in Paper B.

Chapter 5

Laser interaction with near-critical plasmas

The nonlinear nature of the interaction of lasers and plasmas provides opportunity for conversion of the energy in the laser pulse to higher frequency components [85, 86, 87], which are relevant to a range of applications such as diagnostics of phenomena on the attosecond timescale and probing warm dense matter [88, 89, 90]. For weakly relativistic lasers and a steep vacuum-plasma interface, the interface acts as a mirror, although with some electron heating where electron bunches are being launched into the bulk of the plasma [91, 92, 93, 94]. For a smooth density ramp, the electrons may excite plasma oscillations, resulting in the emission of high frequency radiation through Coherent Wake Emission (CWE) [29]. For the interaction of a relativistically intense laser pulse with an overdense plasma, high harmonic radiation arises from the dynamics of the vacuum-plasma interface, which is governed by the balance between the electrostatic force due to charge separation and radiation pressure [30, 31, 85].

The energy accumulated in the electrons at the vacuum-plasma interface puts a limit on the energy that is available to be re-emitted as high-frequency radiation. It turns out that for a relativistically intense laser pulse, the electrons in the sheath formed at the vacuum-plasma boundary can be assigned a common velocity, which to good approximation describes their collective motion. High frequency emission from this sheath occurs at the particular point in time when the electrons coherently move backwards in the opposite direction[1] of the incoming

[1] With respect to a boosted frame. See Section 2.1.

laser pulse. At this point of time, the backwards travelling electric field:

$$E \sim \frac{Q\beta_\perp}{1+\beta_x}$$

exhibits singular behaviour, which gives rise to a sharp pulse containing frequencies beyond the laser frequency. Here, $\vec{\beta} = (\beta_x,\beta_\perp)$ is the velocity of the sheath and Q is its charge. Notice that the γ-factors of the electrons in the sheath are critical to resolve the singularity in the expression for the emitted field. Furthermore, the detailed timing (phase) for the zero-crossing of the transverse velocity for different parts of the layer is important for setting an upper limit for the highest harmonic that can be coherently generated.

Currently, there are at least two theoretical frameworks to describe the generation of high harmonics from relativistic laser-plasma interaction in the overdense regime: The Relativistic Oscillating Mirror (ROM) [30] and Relativistic Electron Spring (RES) [25, 31, 56] model. The former model describes the interaction accurately in the large S-regime (where $S = n_e/a_0 n_c$) and is signified by energy conservation at a point of reflection, whereas the latter describes the dynamics of the electron sheath, in a way that allows for accumulation of energy and consequently higher amplitude of the emitted high harmonics; even reaching relativistic intensities for frequency content in the XUV-regime [25].

This Chapter gives a brief overview of the ROM- and RES-models as well as discusses the scaling of the γ-factor distribution for electrons in the sheath in the RES-model, the energy accumulation in the sheath as well as its thickness, connecting to the topic of Paper D. It is shown that although the RES-model is an S-similar theory, these properties are transient. In particular, energy accumulation in the sheath decays for high a_0, which limits the conversion efficiency of laser energy to high harmonics. Additionally, this Chapter provides an analysis of the micro-dynamics of the sheath based on PIC-simulations, for different regimes of interaction.

5.1 The ROM-model

The Relativistic Oscillating Mirror (ROM) [30] model relies on the assumption that an overdense plasma can be a perceived as a mirror,

with a surface that at every instant of time has a position $x_s(t)$ at which the incoming and reflected transverse fields cancel each other:

$$0 = \vec{E}_{\perp,i}(kx_s(t) - \omega t) + \vec{E}_{\perp,r}(kx_s(t) + \omega t)$$

with $\vec{E}_{\perp,i}$ being the incoming and $\vec{E}_{\perp,r}$ being the reflected field. This is known as a Leontovich boundary condition. Now, consider the reflected field at $x = 0$, corresponding to the phase $\psi = \omega t$. The field at this point is the incoming field at the mirror at a time t' such that $\psi = kx_s(t') + \omega t'$, i.e. the incoming field evaluated at the phase $\tilde{\psi} = 2kx_s(t') - \omega t$:

$$\vec{E}_{\perp,r}(\omega t) = -\vec{E}_{\perp,i}(2kx_s(t') - \omega t).$$

First of all, it is clear from the condition of reflection that the amplitude of the reflected field never can exceed that of the incoming field, which puts a restrictive limit on the relativistic amplitude that is attainable for the high harmonic content of the reflected signal. It may however be noticed, that generalizations of the boundary condition exist, defining the reflection condition in the rest frame of the mirror which consequently reduces the restrictions on the amplitude of the field. Second of all, the frequency content of the reflected signal is determined by the phase compression, which can be seen by considering the effective rate of change for the phase:

$$\frac{\mathrm{d}\tilde{\psi}}{\mathrm{d}t} = \omega \frac{\beta_x(t') - 1}{\beta_x(t') + 1},$$

where β_x is the velocity of the reflection point. The laser frequency is consequently amplified by a factor $(\beta_x(t') - 1)/(\beta_x(t') + 1)$, which can be large for interaction in the relativistic regime. The ROM-model is primarily valid in the parameter region with large S-numbers.

The intensity of high-harmonics is important for their potential use in applications. Regarding this issue, the ROM-model exhibits an amplitude decay of the high-harmonics that scales as $I_n \sim n^{-8/3}$, where n is the wavenumber, which has been observed in simulations [95] and experiments [96, 97], although there also are reports of other scalings [98] for parameter regimes where the mirror approximation shows more limited validity.

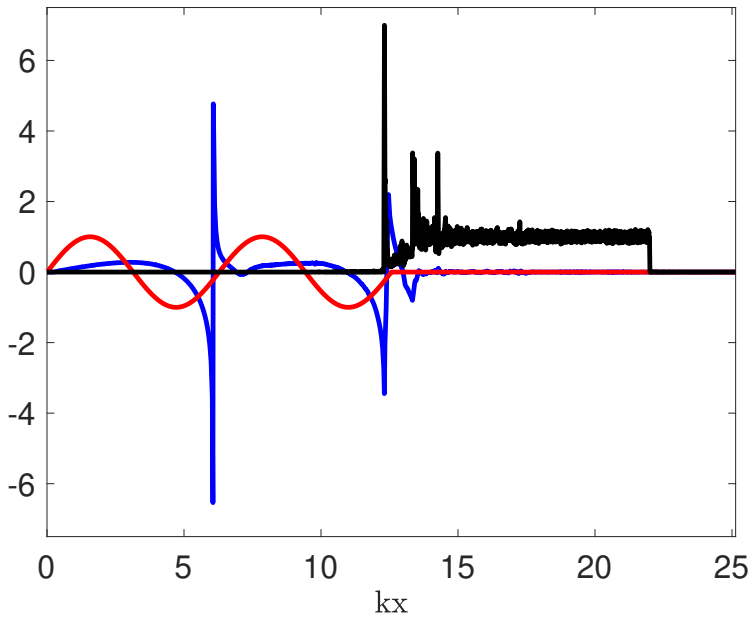

Figure 5.1: Interaction of a plasma with a linearly polarized laser pulse at an angle $\theta = 2\pi/9$ and $S = 0.3/\cos^3\theta$. The incoming laser radiation is shown in red and the reflected signal at a later time is shown in blue, as well as the plasma profile (black) at this time. Quantities are normalized in terms of the amplitude of the incoming laser radiation and the initial plasma density, respectively. Notice that the amplitude of the reflected pulse exceeds that of the incident laser.

5.2 The RES-model

When a laser pulse is incident on an overdense plasma, evidence from simulations show that electrons will organize themselves in a thin sheath at the vacuum-plasma interface, which in the ROM-model is considered to act as a mirror. This turns out to be limiting for the applicability of the model as it does not allow energy to be accumulated in particles and field-structures associated with the sheath. Figure 5.1 shows electric fields and density profiles for laser plasma interaction at $S = 0.3/\cos^3\theta$ and $\theta = 2\pi/9$ angle of incidence. From the Figure, it is evident that the amplitude of the back-radiated high frequency pulse exceeds that of the incident field and can hence not be described by the mirror model. The Relativistic Electron Spring [25, 31, 56] (RES) model provides an alternative interpretation of the physics, by demanding that the incoming laser field is cancelled within a short distance of the vacuum-plasma boundary (of the order of the skin-depth). In particular, it separates the cancellation of the incoming radiation, which occurs through a forward generated field from the backward generated field, which allows energy to be accumulated in the plasma and fields that later is released in an attosecond burst reaching high intensity.

Under the condition of relativistic motion; the electrons forming the sheath at the vacuum-plasma boundary can be modelled with a common velocity $\vec{\beta} = (\beta_x,\beta_y,\beta_z)$. Furthermore, the position of the sheath can be associated with a point x_s which corresponds to piling up a sufficient number of electrons to cancel the incoming radiation. Before stating the RES-equations, notice that by making a Lorentz-transformation in the $\vec{v} = c\sin\theta\,\hat{y}$ direction, laser-plasma interaction at an angle of incidence θ can be treated analogous to that of normal incidence; although with quantities transformed to the moving frame. Further details are given in Section 2.1. In particular, the electrons and ions have an initial velocity $-\vec{v}$ in the transformed frame, which has the effect that when the vacuum-plasma surface is compressed, the unshielded ions give rise to transverse electromagnetic radiation.

For the purpose of illustrating the RES-equations, we consider an incoming laser pulse of the form $\vec{E}(\psi) = E_{y,i}(\psi)\hat{y} + E_{z,i}(\psi)\hat{z}$, where $\psi = \omega t - kx$ is a phase coordinate and $E_{y,i}(\psi)$, $E_{z,i}(\psi)$ are arbitrary functions of phase; interacting with a step-like plasma density profile $n(x) = n_0\Theta(x)$, where $\Theta(x)$ is a step-function and n_0 is the plasma density. In the following time is expressed in terms of ωt, length in kx, density in n_c and field strength in terms of the relativistic field evalu-

ated with respect to the boosted frame. The condition for cancellation of the incoming radiation, known as the RES-condition, can then be expressed as

$$E_{y,i}(x_s - t) + \frac{Q}{2}\left(\sin\theta - \frac{\beta_y}{1-\beta_x}\right) = 0,$$
$$E_{z,i}(x_s - t) - \frac{Q}{2}\frac{\beta_z}{1-\beta_x} = 0,$$

where $Q = n_0 x_s$ is the total charge in the sheath. Based on the relativistic dynamics, it is approximated that the layer moves at the speed of light, i.e. $\beta_x^2 + \beta_y^2 + \beta_z^2 = 1$, resulting in three equations for the four unknowns x_s and $\vec{\beta}$. The system of equations is closed by adding an equation of motion for x_s:

$$\frac{\mathrm{d}x_s}{\mathrm{d}t} = \beta_x.$$

Based on the one-velocity model for electrons in the sheath, the fields therein can be described by:

$$E_x = -(Q-q),$$
$$E_y = (Q-q)\frac{\beta_x\beta_y}{1-\beta_x^2},$$
$$B_y = -(Q-q)\frac{\beta_z}{1-\beta_x^2},$$
$$E_z = (Q-q)\frac{\beta_x\beta_z}{1-\beta_x^2},$$
$$B_z = (Q-q)\frac{\beta_y}{1-\beta_x^2},$$

where q is the amount of electron charge between the vacuum-plasma interface and a position x, inside the layer. Good agreement between the solution of the equations in the RES-model and PIC-simulations is found for the velocity $\vec{\beta}$, as well as for the magnetic fields at the vacuum-plasma interface, as is illustrated in Figure 5.2. In this particular case: $\theta = \pi/7$, $S = 1/\cos^3\theta$ and $\vec{E}(\psi) = \Theta(\psi)a_0(\cos\zeta\sin\psi\,\hat{y} + \sin\zeta\cos\psi\,\hat{z})$ with $a_0 = 1000$ and $\zeta = \pi/3$, with respect to the boosted frame.

From the expression for the back-radiation of the sheath: $E \sim Q\frac{\beta_\perp}{1+\beta_x}$, an emission event is associated with that the longitudinal velocity of the sheath is $\beta_x = -1$. However, this also shows that the

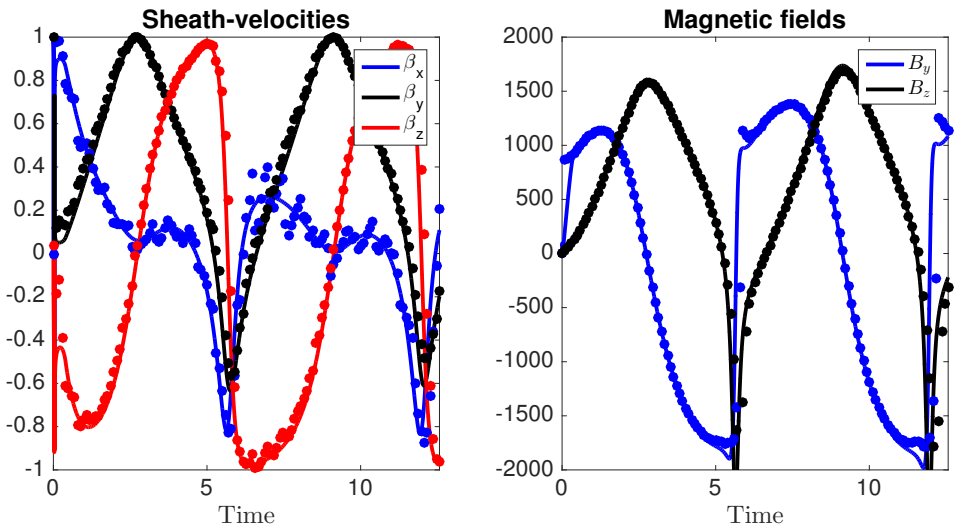

Figure 5.2: Left: Comparison of velocities in the RES-model (lines) and average velocity of sheath from PIC-simulations (dots). Right: Comparison of fields at vacuum-plasma boundary calculated from the RES-model and PIC-simulations, respectively.

assumption that the sheath moves at the speed of light limits the possibility to understand the details of the generated attosecond burst. To resolve this singularity it is necessary to take into account the γ-factors of electrons in the sheath. Notice that finite γ-values give rise to a correction of the velocity:

$$\beta_{x,\gamma} = \beta_x + \mathcal{O}(\gamma^{-2}).$$

If the sheath can be associated with a γ-factor, the peak field can be estimated by $E \sim Q\gamma$. In the following Sections, the micro-dynamics of the sheath is investigated through analytics as well as PIC-simulations, illustrating that a combination of finite γ-effects, retardation as well as small variations in the particle velocities across the sheath play an important role in differentiating which part of the parameter space (values of S, θ) which gives rise to radiation spectra of different properties as well as their dependence on the relativistic amplitude a_0.

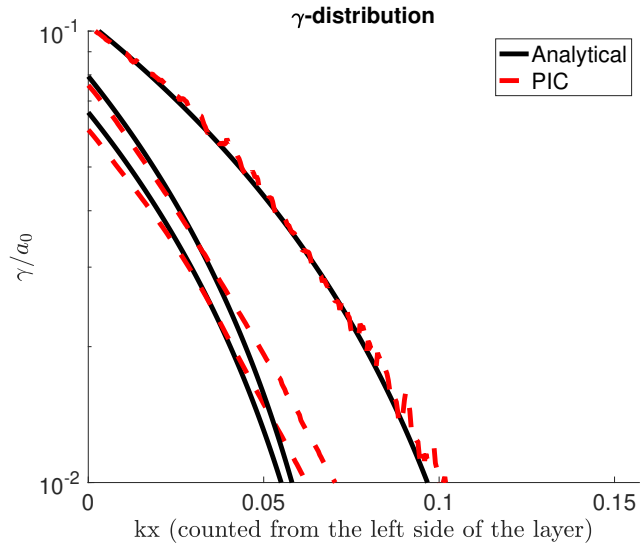

Figure 5.3: Comparison of γ-factor distribution from PIC-simulations and analytical expression in terms of RES-parameters and the layer thickness.

5.3 γ-factor distribution

By assuming that the electron sheath has a constant density, the vector potential, arising from the electromagnetic fields inside the sheath, stated in Section 5.2, can be calculated. By using the conservation of canonical momentum, this implies a γ-factor distribution in the sheath:

$$\gamma = \frac{Q\Delta x}{1-\beta_x^2}\frac{\delta x^2}{2} \tag{5.1}$$

where $\delta x = (x_s - x)/\Delta x$ and Δx is the thickness of the sheath. In Figure 5.3, the γ-factor distribution from this formula is compared to that from PIC-simulations, indicating good agreement.

A problem with the analytical expression (5.1) is that it is not entirely independent from PIC-simulations, which are used to determine the thickness of the sheath. An alternative approach to determine the scale for γ-factors in the layer, conducted by Serebryakov *et al* [99], has been to calculate a γ-factor, by identifying the layer with an electron experiencing an average field with respect to all electrons in the layer. However, as electrons are continuously added and removed from the sheath, the γ-factor of such an average electron is difficult to connect

to the scale for γ of actual electrons in the sheath, which limits the applicability of the model. The problem of determining the thickness is closely connected to determining the energy-flow into the plasma, but which turns out to be a complicated problem, which is discussed in the following Sections and in Paper D. The problem of determining the thickness may also be expressed in terms of compression of the sheath, although the compression equation neither directly provides a way to determine the a_0 scaling of Δx. However, it is clear that determining the scaling of Δx is critical in determining the scale of the γ-distribution and in particular, if Δx has a non-constant dependency on a_0, it means that the energy-scale of the electron sheath cannot be described by S-similarity theory.

5.4 Thickness of the electron sheath

In this Section, we shed light on a number of approaches to determine the thickness of the electron sheath for laser-plasma interaction in the moderately overdense regime. First of all, if heating, perceived in terms of energy transport through particles leaving the sheath and moving further into the bulk plasma, is neglected – the energy in fields and particles inside the plasma becomes

$$W = \frac{Q^2 \Delta x}{2(1-\beta_x^2)}.$$

Consequently, the thickness of the sheath can be determined if the energy is known. To calculate the energy that is delivered from the laser to the particles and fields inside the plasma; the energy-flow across the vacuum-plasma boundary:

$$\frac{\mathrm{d}W}{\mathrm{d}t} = -\tilde{\beta}_x u(x_{\mathrm{vp}},t) + S_x(x_{\mathrm{vp}},t)$$

should be integrated, where x_{vp} is the position of the vacuum-plasma interface, u is the electromagnetic energy density, $\vec{S}$ is the Poynting vector and $\tilde{\beta}_x$ is the velocity of an electron at the vacuum-plasma interface. With the fields in Section 5.2 and a $\tilde{\beta}_x$ that is only modified due to finite γ-factor, the rate of change is of the order γ^{-2}, arising from a proportionality towards $(\beta_x - \tilde{\beta}_x)$. However, as the assumption that the sheath moves at the speed of light merely is an approximation that is acceptable for the purpose of integrating its motion, comparing

it to other velocities close to the speed of light is more questionable, which highlights that effects of the order of the layer thickness, e.g. retardation and deviations from the one-velocity model also may play a critical role in determining the energy flow.

To investigate the relation between the electron motion in the sheath and single-velocity models such as the RES-model, we express the equations of motion for electrons with reference to the field-expressions in Section 5.2, evaluated using the velocity of an electron at the vacuum-plasma interface. Denoting the difference in velocity/fields for an electron positioned with a total charge q to the left of it by $\Delta\vec{\beta}$ and $\Delta\vec{E}$, $\Delta\vec{B}$; the equations of motion take the form

$$\begin{aligned}
\frac{\mathrm{d}p_x}{\mathrm{d}t} &= \Delta E_x + \Delta B_z\beta_y + B_z\Delta\beta_y - \\
&\quad \Delta B_y\beta_z - B_y\Delta\beta_z - \frac{Q-q}{\gamma_{\max}^2(1-\beta_x^2)}, \\
\frac{\mathrm{d}p_y}{\mathrm{d}t} &= \Delta E_y - \Delta B_z\beta_x - B_z\Delta\beta_x, \\
\frac{\mathrm{d}p_z}{\mathrm{d}t} &= \Delta E_z + \Delta B_y\beta_x + B_y\Delta\beta_x,
\end{aligned}$$

where $\gamma_{\max}$ is the γ-factor for the electron at the vacuum-plasma boundary. From these equations it is evident that even the primary motion (i.e. the path corresponding to the sheath-velocity) is generated by effects such as retardation and variations in velocities across the sheath, which complicates the problem and shows that the velocity dispersion and RES-velocity need to be solved for together.

The layer-thickness may also be addressed separately from the energy-flow across the vacuum-plasma boundary. The evolution of the layer thickness can then be interpreted in terms of compression due to variations of β_x across the layer. This approach has the benefit that it separates the evolution of the layer thickness and energy in the sheath, which may be beneficial to describe heating processes. An equation for the evolution for the density can be obtained by taking a time-derivative of the relation $\mathrm{d}q/n = \mathrm{d}x$, where $\mathrm{d}x$ is an infinitesimal part of the layer:

$$\frac{\mathrm{d}n}{\mathrm{d}t} = -\frac{\partial\beta_x}{\partial q}n^2,$$

which connects the density evolution to the gradient of β_x. To analyze the β_x-distribution, it is necessary to solve the equations of motion,

which as pointed out is a complicated problem. However, observe that

$$\frac{\partial \beta_x}{\partial q} = \frac{1}{\gamma}\left(\frac{\partial \Delta p_x}{\partial q} - \Delta p_x \frac{\partial \log \gamma}{\partial q}\right) := \frac{K(q)}{\gamma},$$

where $\Delta p_x = p_x - p_{x,s}$ and $p_{x,s}$ is the momentum evaluated using a single-velocity model for the electrons in the sheath. Also, if $\Delta p_x = \tilde{K}(Q-q)$, it turns out that $\tilde{K} = K$ and

$$\frac{\mathrm{d}n}{\mathrm{d}t} = -\frac{\tilde{K}}{\gamma} n^2.$$

To obtain a closed expression for n, we make the assumption that the thickness can be calculated from $\Delta x = Q/n$ and evaluate γ at the vacuum-plasma interface. In that case

$$\frac{\mathrm{d}n}{\mathrm{d}t} = -\frac{2(1-\beta_x^2)\tilde{K}}{Q^2} n^3,$$

which has the solution:

$$\frac{1}{n(t)^2} = \frac{1}{\tilde{n}^2} + \int_{\tilde{t}}^{t} \frac{2(1-\beta_x^2)\tilde{K}}{Q^2}\,\mathrm{d}t,$$

where $\tilde{n}$ is the density at time $\tilde{t}$. As $\tilde{K}$ depends on a_0 through $1/\gamma^2$, it appears as if $n(t)$ has a limit for large a_0. However, such analysis is complicated by that a small inaccuracy in $\tilde{K}$ makes the difference between a high density and an infinite density.

Finally, a tractable path to address the scaling of the layer thickness with a_0, is by considering the balance between the radiation pressure and electrostatic force due to charge separation. This translates into estimating the layer thickness with the skin depth, which provides $\Delta x \sim a_0^{-0.5}$. With such scaling it follows that $\gamma \sim a_0^{0.5}$ and $W \sim a_0^{1.5}$. In Paper D, this is indicated to be an acceptable approximation in a range of cases. From this it follows that the energy range for electrons in the sheath grows with a_0, although at a slower pace than what is predicted from S-similarity theory.

5.5 Radiation generation in the RES-model

We now consider the emission event for the electron sheath. High harmonics are generated from the laser plasma interaction when the

sheath is moving at a velocity close to the speed of light in the negative x-direction. An element of charge $\mathrm{d}q$ in the sheath, positioned at $x(t)$, emits in the phase $\psi = x(t) + t$ with an amplitude described by

$$\mathrm{d}E_y(\psi) = \frac{\mathrm{d}q}{2}\frac{\beta_y(t)}{1+\beta_x(t)}.$$

If $\gamma \gg 1$ and as $\beta_y \approx 0$: $\beta_x = -\sqrt{1-1/\gamma^2-\beta_y^2} \approx -1 + 1/2\gamma^2 + \beta_y^2/2$. Furthermore, approximating $\beta_y \approx (\mathrm{d}\beta_y/\mathrm{d}t)(t-t_e)$, where t_e is such that $\beta_y = 0$, it follows that

$$\mathrm{d}E_y(\psi) = \mathrm{d}q\frac{\alpha\gamma^2(t-t_e)}{1+\gamma^2\alpha^2(t-t_e)^2},$$

where $\alpha = \mathrm{d}\beta_y/\mathrm{d}t$. Defining $\psi_0 = x(t_e) + t_e$, i.e. the phase associated with $\beta_y = 0$, and observing that $\psi - \psi_0 = (1+\beta_x)(t-t_e) \approx (t-t_e)/2\gamma^2$, the field can be approximated around the point $\beta_y = 0$ by:

$$\mathrm{d}E_y(\psi) = \mathrm{d}q\frac{2\alpha\gamma^4(\psi-\psi_0)}{1+4\gamma^6\alpha^2(\psi-\psi_0)^2}.$$

The total electric field becomes

$$E_y(\psi) = \int \frac{2\alpha\gamma^4(\psi-\psi_0)}{1+4\gamma^6\alpha^2(\psi-\psi_0)^2}\mathrm{d}q,$$

where the details of ψ_0 are not resolved in our model. Taking the Fourier-transform of this expression gives

$$\hat{E}_y(k) = i\sqrt{\frac{\pi}{2}}\int \frac{1}{2\gamma^2\alpha}e^{ik\psi_0 - k/2\alpha\gamma^3}\mathrm{d}q.$$

To evaluate the Fourier spectrum it is therefore necessary to know γ, α and ψ_0 for each element of the sheath. Regarding the frequency cutoff, denoted k, for high harmonics generated from the interaction:

$$k \approx 2\pi/\Delta\psi_0,$$

where $\Delta\psi_0$ is the difference between the maximum and minimum phase for the occurence of $\beta_y = 0$ for electrons in the layer. This range is determined by the delay between emission from different parts of the layer, in combination with retardation effects. To reach the highest frequencies it is beneficial if the delay is such that it cancels the destructive interference from retardation due to the layer thickness.

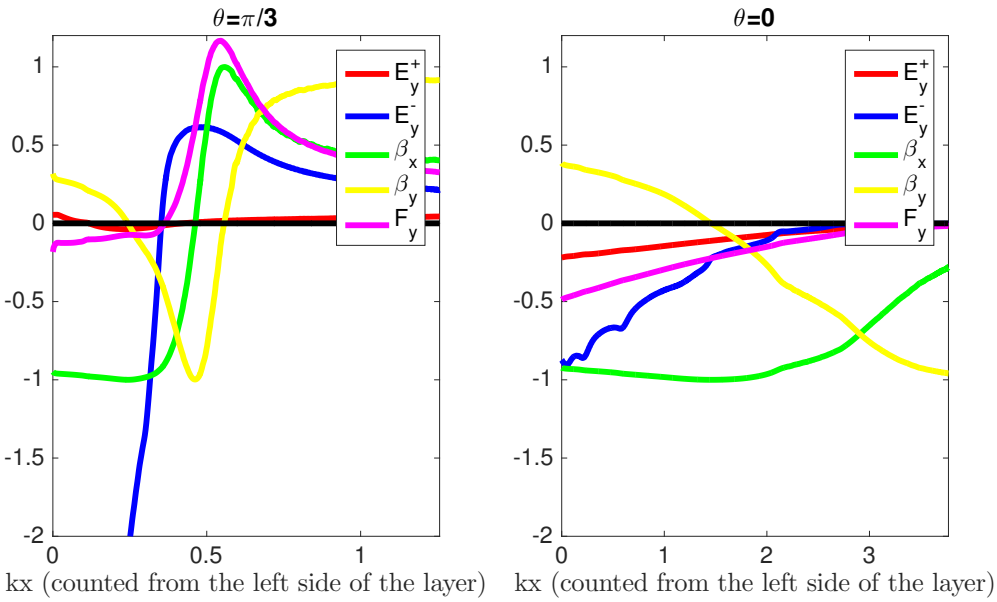

Figure 5.4: Right- and leftmoving electric field E_y^+, E_y^-, transverse force F_y and particle velocities β_x, β_y at an instant of time during emission of attosecond burst for linearly polarized laser light interacting with a plasma such that $S = 0.3$, $\theta = 0$ and $S = 0.3/\cos^3\theta$, $\theta = \pi/3$ respectively.

5.6 Microdynamics during radiation emission in sheath

As described by Gonoskov *et al* [31], the parameter space for interaction of linearly polarized laser light with a plasma of constant density has three distinct parameter regions; depending on the number of times the transverse velocity turns zero (zero, one or two) for each optical cycle. The transverse velocity may either cross zero and thereafter assume the opposite sign or barely touch zero. The latter situation, which occur for $S \approx 0.5/\cos^3\theta$, $\theta \approx \pi/3$, is known to lead to optimal conditions for generation of coherent high harmonics. Here, we use PIC-simulations to illustrate how the dynamics of the electron layer is different in the respective regimes of interaction.

Regarding the emission parameter α, notice that $\alpha = F_y/\gamma$, where the force term takes the form

$$F_y = 2E_y^+ + \frac{E_y^- - E_y^+}{2\gamma^2},$$

where E_y^+ is the right-moving and E_y^- is the left-moving part of the electric field. If $\gamma \gg 1$, this means that the incoming field plays the most important role for the transverse acceleration when the transverse velocity is close to zero, although the outgoing field may play a significant role in reducing the transverse momentum so that the transverse velocities approach zero. To gain an understanding of the force on the electrons when the transverse velocity is close to zero, observe that

$$E_y^+ \approx E_{y,i} + \frac{Q\sin\theta}{2}.$$

If this quantity is negative, the transverse velocity crosses zero and switches sign. Commonly, the electrons closest to the RES-point cross zero first and therefore generate a high intensity field that slowly traverses the sheath. An interesting behaviour occurs if $E_y^+ \approx 0$, which corresponds to that the field moving onto the plasma is too weak to perform substantial transverse acceleration. In this case, the zero crossing occurs more slowly and the reduction of transverse momentum is more driven by interaction of the electrons with the left-moving attosecond burst generated by electrons whose transverse velocity already has crossed zero. This is illustrated in Figure 5.4, showing a snapshot of the left- and right-travelling fields, transverse force and velocity for the

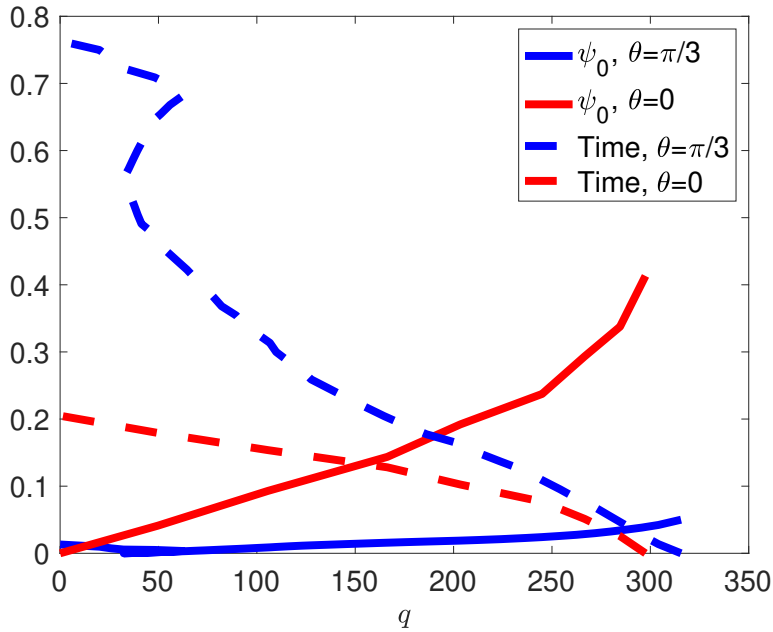

Figure 5.5: Phase (ψ_0) calculated as a function of the charge q, parametrizing the emission from different parts of the layer. Also shows time for emission as a function of q, indicating that although the case with $S = 0.3/\cos^3\theta$, $\theta = \pi/3$ emits for a longer time, the synchronization of zero-crossing for the transverse velocity with the partially generated attosecond burst leads to a smaller range for ψ_0 than in the case with $S = 0.3$, $\theta = 0$.

electrons inside the sheath for two different cases: $S = 0.3$, $\theta = 0$ and $S = 0.3/\cos^3\theta$, $\theta = \pi/3$. To indicate the implications of the different dynamics for the two cases, Figure 5.5 shows ψ_0 as a function of the charge coordinate q. The figure indicates that although the emission event for the case with $S = 0.3/\cos^3\theta$, $\theta = \pi/3$ takes longer time, the coordination leads to a smaller spread for ψ_0 than in the case with $S = 0.3$, $\theta = 0$.

Acknowledgements

I am grateful to my supervisor Mattias Marklund, and to Arkady Gonoskov for always being supporting and providing guidance in the endeavours which constitute this thesis. Furthermore, throughout this project I have had the opportunity to work with several excellent people contributing to a creative and friendly work environment. In addition to the people already mentioned, I would like to recognize Tim Dubois, Tünde Fülöp and Evangelos Siminos for good collaboration in projects, as well as Joel Magnusson and Stefan Buller for providing occasional distractions from the tasks needed to be done. Finally, I would like to extend my gratitude to my family, especially my girlfriend Qian Wang, for making every step along the path to this thesis a happy moment.

Benjamin Svedung Wettervik, 2019

Bibliography

[1] T. H. Maiman, *Stimulated optical radiation in ruby*, Nature 187, 493-494, 1960.

[2] D. Strickland, G. Mourou, *Compression of amplified chirped optical pulses*, Optics Communications 56, 3, 219-221, 1985.

[3] Vulcan: `www.clf.stfc.ac.uk`.

[4] BELLA: `http://www2.lbl.gov/publicinfo/newscenter/features/2008/apr/af-bella.html`.

[5] XCELS: `www.xcels.iapras.ru`.

[6] E. Esarey, C. B. Schroeder, W. P. Leemans, *Physics of laser-driven plasma-based electron accelerators*, Rev. Mod. Phys. 81, 3, 1229-1285, 2009.

[7] H. Daido, M. Nishiuchi, A. S. Pirozhkov, *Review of laser-driven ion sources and their applications*, Rev. Prog. Phys 75, 5, 056401, 2012.

[8] B. Dromey, M. Zepf, A. Gopal, K. Lancaster, M. S. Wei, K. Krushelnick, M. Tatarakis, N. Vakakis, S. Moustaizis, R. Kodama, M. Tampo, C. Stoeckl, R. Clarke, H. Habara, D. Neely, S. Karsch, P. Norreys, *High harmonic generation in the relativistic limit*, Nat. Phys. 2, 456-459, 2006.

[9] M. Cole, K. T. Behm, E. Gertsmayr, T. G. Blackburn, J. C. Wood, C. D. Baird, M. J. Duff, C. Harvey, A. Ilderton, A. S. Joglekar, K. Krushenick, S. Kuschel, M. Marklund, P. McKenna, C. D. Murphy, K. Poder, C. P. Ridgers, G. M. Samarin, G. Sarri, D. R. Symes, A. G. R. Thomas, J. Warwick, M. Zepf, Z. Najmudin, S. P. D. Magnles, *Experimental evidence of radiation reaction in*

the collision of a high-intensity laser pulse with a laser-wakefield accelerated electron beam, Phys. Rev. X 8, 1, 011020, 2018.

[10] K. Poder, M. Tamburini, G. Sarri, A. Di Piazza, S. Kuschel, C. D. Baird, K. Behm, S. Bohlen, J. M. Cole, D. J. Corvan, M. Duff, E. Gerstmayr, C. H. Keitel, K. Krushelnick, S. P. D. Mangles, P. McKenna, C. D. Murphy, Z. Najmudin, C. P. Ridgers, G. M. Samarin, D. R. Symes, A. G. R. Thomas, J. Warwick, M. Zepf, *Experimental Signatures of the Quantum Nature of Radiation Reaction in the Field of an Ultraintense Laser*, Phys. Rev. X 8, 031004, 2018.

[11] A. Gonoskov, M. Marklund, *Radiation-dominated particle and plasma dynamics*, Physics of Plasmas 25, 093109, 2018.

[12] J. M. Dawson, *Particle simulation of plasmas*, Rev. Mod. Phys. 55, 2, 403-447, 1983.

[13] C. K. Birdsall, A. B. Langdon, *Plasma physics via computational simulation*, McGraw-Hill, 1985.

[14] ELI: `www.eli-laser.eu`.

[15] C. Z. Cheng, G. Knorr, *The integration of the Vlasov equation in configuration space*, J. Comp. Phys. 22, 3, 330-351, 1976.

[16] D. Keefe, *Inertial confinement fusion*, Ann. Rev. Nucl. Part. Sci. 32, 391, 1982.

[17] R. Orecchia,A. Zurlo, A. Loasses, M. Krengli, G. Tosi, S. Zurrida, P. Zucali, U. Veronesi, *Particle beam therapy (hadrontherapy): basis for interest and clinical experience*, European Journal of Cancer 34, 4, 459-468, 1998.

[18] U. Linz. J. Alonso, *What will it take for laser driven proton accelerators to be applied to tumor therapy?*, Phys. Rev. ST Accel. Beams 10, 094801, 2007.

[19] J. M. Cole, J. C. Wood, N. C. Lopes, K. Poder, R. L. Abel, S. Alatabi, J. S. J. Bryant, A. Jin, S. Kneip, K. Mecseki, D. R. Symes, S. P. D. Mangles, Z. Najmudin, *Laser-wakefield accelerators as hard x-ray sources for 3D medical imaging of human bone*, Scientific Reports 5, 13244, 2015.

[20] J. Wenz, S. Schleede, K. Khrennikov, M. Bech, P. Thibault, M. Heigoldt, F. Pfeiffer, S. Karsch, *Quantitative X-ray phase-contrast microtomography from a compact laser-driven betatron source*, Nature Communications 6, 7568, 2015.

[21] SLAC: `https://www6.slac.stanford.edu/`.

[22] L. Evans, P. Bryant, *LHC machine*, Journal of Instrumentation, 3(08):S08001, 2008.

[23] W. P. Leemans, B. Nagler, A. J. Gonsalves, C. Toth, K. Nakamura, C. G. R. Geddes, E. Esarey, C. B. Schroeder, S. M. Hooker, *GeV electron beams from a centimetre-scale accelerator*, Nature Phys. 2, 696-699, 2006.

[24] T. Tajima, J. M. Dawson, *Laser electron accelerator*, Phys. Rev. Lett. 43, 4, 267-270, 1979.

[25] T. Blackburn, A. Gonoskov, M. Marklund, *Relativistically intense XUV radiation from laser-illuminated near-critical plasmas*, Phys. Rev. A 98, 023421, 2018.

[26] V. I. Veksler, *Coherent principle of acceleration of charged particles* Proc. CERN Symp. of High Energy Accelerators and Pion Physics, Geneva, Switzerland, 1956.

[27] A. Macchi, M. Borgesi, M. Passoni, *Ion acceleration by superintense laser-plasma interaction*, Rev. Mod. Phys. 85, 2, 751-793, 2013.

[28] H. Zhirong, K. Kwang-Je, *Review of x-ray free-electron laser theory*, Phys. Rev. ST Accel. Beams 10, 034801, 2007.

[29] F. Quere, C. Thaury, P. Monot, S. Dobosz, Ph. Martin, J.-P. Geindre, P. Audebert, *Coherent wake emission of high-order harmonics from overdense plasmas*, Phys. Rev. Lett. 96, 125004, 2006.

[30] S. Gordienko, A. Pukhov, O. Shorokhov, T. Baeva, *Relativistic doppler effect: universal spectra and zeptosecond pulses*, Phys. Rev. Lett. 93, 115002, 2004.

[31] A. A. Gonoskov, A. V. Korzhimanov, A. V. Kim, M. Marklund, A. M. Sergeev, *Ultra-relativistic nanoplasmonics as a route towards*

extreme-intensity attosecond pulses, Phys. Rev. E 84, 4, 046403, 2011.

[32] P. Debye, E. Hückel, *The theory of electrolytes. I. Lowering of freezing point and related phenomena*, Physikalische Zeitschrift 24, 185-206, 1923.

[33] A. Macchi, *A superintense laser-plasma interaction theory primer*, Wiley, 2013.

[34] J. D. Jackson, *Classical electrodynamics*, 3rd ed., Wiley, 1998.

[35] A. A. Vlasov. J. Phys. U.S.S.R., 9, 25, 1945.

[36] C. Cercignani, V. Gerasimenko, D. Petrina, *Many-particle dynamics and kinetic equations*, Mathematics and Its Applications, Springer, 1997.

[37] A. Einstein, *Zur Elektrodynamik bewegter Körper*, Annalen der Physik 17: 891, 1905.

[38] A. Bourdier, *Oblique incidence of a strong electromagnetic wave on a cold inhomogeneous electron plasma. Relativistic effects*, The Physics of Fluids 26, 1804, 1983.

[39] L. D. Landau, E. M. Lifshitz, *The classical theory of fields*, Elsevier, 1975.

[40] A. Gonoskov, S. Bastrakov, E. Efimenko, A. Ilderton, M. Marklund, I. Meyerov, A. Muraviev, A. Sergeev, I. Surmin, E. Wallin, *Extended particle-in-cell schemes for physics in ultrastrong laser fields: Review and developments*, Phys. Rev. E 92, 2, 023305, 2015.

[41] J. D. Lawson, Rutherford Laboratory report RL-75-043, 1975.

[42] T. Plettner, R. L. Byer, E. Colby, B. Cowan, C. M. S. Sears, J. E. Spencer, R. H. Siemann, *Visible-laser acceleration of relativistic electrons in a semi-infinite vacuum*, Phys. Rev. Lett. 95, 134801, 2005.

[43] K. I. Popov, V. Y. Bychenkov, W. Rozmus, R. D. Sydora, S. S. Bulanov, *Vacuum electron acceleration by tightly focused laser pulses with nanoscale targets*, Physics Of Plasmas 16, 053106, 2016.

[44] D. Bauer, P. Mulser, W. H. Steeb, *Relativistic ponderomotive force, uphill acceleration, and transition to chaos*, Phys. Rev. Lett. 75, 4622, 1995.

[45] F. Cattani, A. Kim, D. Anderson, M. Lisak, *Threshold of induced transparency in the relativistic interaction of an electromagnetic wave with overdense plasmas*, Phys. Rev. E 62, 1, 1234-1237, 2000.

[46] E. Siminos, M. Grech, S. Skupin, T. Schlegel, V. T. Tikhonchuk, *Effect of electron heating on self-induced transparency in relativistic-intensity laser-plasma interactions*, Phys. Rev. E 86, 056404, 2012.

[47] A. V. Korzhimanov, A. A. Gonoskov, A. V. Kim, A. M. Sergeev, *Interaction of relativistically strong electromagnetic waves with a layer of overdense plasma*, JETP 105, 4, 675-686, 2007.

[48] E. Siminos, M. Grech, B. Svedung Wettervik, T. Fülöp, *Kinetic and finite ion mass effects on the transition to relativistic self-induced transparency in laser-driven ion acceleration*, New Journal of Physics 19, 12, 123042, 2017.

[49] A. Pukhov, S. Gordienko, S. Kiselev, I. Kostyukov, *The bubble regime of laser-plasma acceleration: monoenergetic electrons and the scalability*, Plasma Physics and Controlled Fusion 46, 12B, 2004.

[50] S. Gordienko, A. Pukhov, *Similarity for ultra-relativistic laser plasmas and the optimal acceleration regime*, arXiv:physics/0411099, 2004.

[51] V. Malka, J. Faure, Gauduel, E. Y. A., Lefebvre, A. Rousse, and K. T. Phuoc, *Principles and applications of compact laser-plasma accelerators*, Nat. Phys. 4, 447, 2008.

[52] P. Mora, T. M. Antonsen, *Electron cavitation and acceleration in the wake of an ultraintense, self-focused laser pulse*, Phys. Rev. E 53, R2068, 1996.

[53] T. Tajima, M. Cavenago, *Crystal x-ray accelerator*, Phys. Rev. Lett. 59, 1440, 1987.

[54] X. Zhang, T. Tajima, D. Farinella, Y. Shin, G. Mourou, J. Wheeler, P. Taborek, P. Chen, F. Dollar, B. Shen, *Particle-in-cell simulation of x-ray wakefield acceleration and betatron radiation in nanotubes*, Phys. Rev. Accel. Beams 19, 10, 101004, 2016.

[55] S. Hakimi, T. Nguyen, D. Farinella, C. K. Lau, H.-Y. Wang, P. Taborek, F. Dollar, T. Tajima, *Wakefield in solid state plasma with the ionic lattice force*, Physics of Plasmas 25, 023112, 2018.

[56] A. A. Gonoskov, *Theory of relativistic radiation reflection from plasmas*, Physics of Plasmas 25, 013108, 2018.

[57] A. Gonoskov, *Ultra-intense laser-plasma interaction for applied and fundamental physics*, Ph.D. thesis, Umeå University, 2013.

[58] B. Svedung Wettervik, A. Gonoskov, M. Marklund, *Prospects and limitations of wakefield acceleration in solids*, Physics of Plasmas 25, 013107, 2018.

[59] A. Macchi, Federica Cattani, T. V. Liseykina, F. Cornolti, *Laser acceleration of ion bunches at the front surface of overdense plasmas*, Phys. Rev. Lett. 94, 165003, 2005.

[60] A. P. L. Robinson, P. Gibbon, M. Zepf, S. Kar, R. G. Evans, C. Bellei, *Relativistically correct hole-boring and ion acceleration by circularly polarized laser pulses*, Plasma Phys. Controlled Fusion 51, 024004, 2009.

[61] D. Haberberger, S. Tochitsky, F. Fiuza, C. Gong, R. A. Fonseca, L. O. Silva, W. B. Mori, C. Joshi, *Collisionless shocks in laser-produced plasma generate monoenergetic high-energy proton beams*, Nat. Phys. 8, 95-99, 2012.

[62] F. Fiuza, A. Stockem, E. Boella, R. A. Fonseca, L. O. Silva, D. Haberberger, S. Tochitsky, C. Gong, W. B. Mori, C. Joshi, *Laser-driven shock acceleration of monoenergetic ion beams*, Phys. Rev. Lett. 109, 215001, 2012.

[63] S. S. Moiseev, R. Z. Sagdeev, *Collisionless shock waves in a plasma in weak magnetic fields*, Journal of Nuclear Energy Part C 5, 1, 32-47, 1963.

[64] A. Pak, S. Kerr, N. Lemos, A. Link, P. Patel, F. Albert, L. Divol, B. B. Pollock, D. Haberberger, D. Froula, M. Gauthier, S. H. Glenzer, A. Longman, L. Manzoor, R. Fedosejevs, S. Tochitsky, C. Joshi, F. Fiuza, *Collisionless shock acceleration of narrow energy spread ion beams from mixed species plasmas using 1 μm lasers*, Phys. Rev. Accel. Beams 21, 103401, 2018.

[65] T. Esirkepov, M. Borghesi, S. V. Bulanov, G. Mourou, T. Tajima, *Highly efficient relativistic-ion generation in the laser-piston regime*, Phys. Rev. Lett. 92, 175003, 2004.

[66] F. Mackenroth, A. Gonoskov, and M. Marklund, *Chirped-standing-wave acceleration of ions with intense lasers*, Phys. Rev. Lett. 117, 104801, 2016.

[67] B. Svedung Wettervik, T. C. DuBois, T. Fülöp, *Vlasov modelling of laser-driven collisionless shock acceleration of protons*, Physics of Plasmas, 23, 5, 053103, 2016.

[68] K. Yee, *Numerical solution of initial boundary value problems involving maxwell's equations in isotropic media*, IEEE Transactions on Antennas and Propagation 14, 3, 302-307, 1966.

[69] J. P. Boris, *Relativistic plasma simulation-optimization of a hybrid code*, Proceeding of Fourth Conference on Numerical Simulations of Plasmas, 1970.

[70] M. Chen, E. Cormier-Michel, C. Geddes, D. Bruhwiler, L. Yu, E. Esarey, C. Schroeder, W. Leemans, *Numerical modeling of laser tunneling ionization in explicit particle-in-cell codes*, Journal of Computational Physics 238, 220-228, 2013.

[71] F. Peano, M. Marti, L. O. Silva, G. Copp, *Statistical kinetic treatment of relativistic binary collisions*, Phys. Rev. E 79, 025701, 2009.

[72] M. Tamburini, F. Pegoraro, A. Di Piazza, C. H. Keitel, A. Macchi, *Radiation reaction effects on radiation pressure acceleration*, New Journal of Physics 12, 123005, 2010.

[73] C. Ridgers, J. Kirk, R. Duclous, T. Blackburn, C. Brady, K. Bennett, T. Arber, A. Bell, *Modelling gamma-ray photon emission and pair production in high-intensity laser-matter interactions*, Journal of Computational Physics 260, 273-285, 2014.

[74] M. Shoucri, ed., *Eulerian codes for the numerical solution of the kinetic equations of plasmas*, Nova Science Publishers, New York, 2011.

[75] C. Z. Cheng, G. Knorr, *The integration of the Vlasov equation in configuration space*, Journal of Computational Physics 22, 330-351, 1976.

[76] N. Besse, G. Latu, A. Ghizzo, E. Sonnendrücker, P. Bertrand, *A wavelet-MRA-based adaptive semi-Lagrangian method for the relativistic Vlasov-Maxwell system*, Journal of Computational Physics 227, 16, 7889-7916, 2008.

[77] A. Grassi, L. Fedeli, A. Sgattoni, A. Macchi, *Vlasov simulation of laser-driven shock acceleration and ion turbulence*, Plasma Physics and Controlled Fusion, 58, 3, 2016.

[78] E. Sonnendrücker, J. Roche, P. Bertrand, A. Ghizzo, *The semi-Lagrangian method for the numerical resolution of the Vlasov equation*, Journal of Computational Physics, 149, 2, 1999.

[79] N. J. Sircombe, T. D. Arber, *VALIS: A split-conservative scheme for the relativistic 2D Vlasov-Maxwell system*, Journal of Computational Physics 228, 13, 4773-4788.

[80] A. Ghizzo, F. Huot, P. Bertrand, *A non-periodic 2D semi-Lagrangian Vlasov code for laser-plasma interaction on parallel computer*, Journal of Computational Physics 186, 1, 47-69, 2003.

[81] S. Von Alfthana, D. Pokhotelovab, Y. Kempfab, S. Hoilijokiab, I. Honkonenab, A. Sandroosa, M. Palmrotha, *Vlasiator: First global hybrid-Vlasov simulations of Earth's foreshock and magnetosheath*, Journal of Atmospheric and Solar-Terrestrial Physics 120, 24-35, 2014.

[82] J. Juno, A. Hakim, J. TenBarge, E. Shi, W. Dorland, *Discontinuous Galerkin algorithms for fully kinetic plasmas*, Journal of Computational Physics 353, 110-147, 2018.

[83] J. Hittinger, J. Banks, *Block-structured adaptive mesh refinement algorithms for Vlasov simulation*, Journal of Computational Physics 241, 118-140, 2013.

[84] B. Svedung Wettervik, T. C. DuBois, E. Siminos, T. Fülöp, *Relativistic Vlasov-Maxwell modelling using finite volumes and adaptive mesh refinement*, The European Physical Journal D 71, 6, 156-171, 2017.

[85] B. Dromey, S. Rykovanov, M. Yeung, R. Hörlein, D. Jung, D. C. Gautier, T. Dzelzainis, D. Kiefer, S. Palaniyppan, R. Shah, J. Schreiber, H. Ruhl, J. C. Fernandez, C. L. S. Lewis, M. Zepf, B. M. Hegelich, *Coherent synchrotron emission from electron nanobunches formed in relativistic laser-plasma interactions*, Nature Physics volume 8, 804-808, 2012.

[86] A. Borot, A. Malvache, X. Chen, A. Jullien, J.-P. Geindre, P. Audebert, G. Mourou, F. Quere, R. Lopez-Martens, *Attosecond control of collective electron motion in plasmas*, Nature Physics 8, 416-421, 2012.

[87] D. Kormin, A. Borot, G. Ma, W. Dallari, B. Bergues, M. Aladi, I. B. Földes, and L. Veisz, *Spectral interferometry with waveform-dependent relativistic high-order harmonics from plasma surfaces*, Nature Communications 9, 4992, 2018.

[88] S. Dobosz, G. Doumy, H. Stabile, P. D'Oliveira, P. Monot, F. Reau, S. Hüller, P. Martin, *Probing hot and dense laser-induced plasmas with ultrafast XUV pulses*, Phys. Rev. Lett. 95, 025001, 2005.

[89] E. Galtier, F. B. Rosmej, T. Dzelzainis, D. Riley, F. Y. Khattak, P. Heimann, R. W. Lee, A. J. Nelson, S. M. Vinko, T. Whitcher, J. S. Wark, T. Tschentscher, S. Toleikis, R. R. Fäustlin, R. Sobierajski, M. Jurek, L. Juha, J. Chalupsky, V. Hajkova, M. Kozlova, J. Krzywinski, B. Nagler, *Decay of crystalline order and equilibration during the solid-to-plasma transition induced by 20-fs microfocused 92-eV free-electron-laser pulses*, Phys. Rev. Lett. 106, 164801, 2011.

[90] F. Krausz, M. Ivanov, *Attosecond physics*, Rev. Mod. Phys. 81, 163, 2009.

[91] D. W. Forslund, J. M. Kindel, Kenneth Lee, E. L. Lindman, R. L. Morse, *Theory and simulation of resonant absorption in a hot plasma*, Phys. Rev. A 11, 679, 1975.

[92] F. Brunel, *Not-so-resonant, resonant absorption*, Phys. Rev. Lett. 59, 52, 1987.

[93] S. C. Wilks, W. L. Kruer, M. Tabak, A. B. Langdon, *Absorption of ultra-intense laser pulses*, Phys. Rev. Lett. 69, 1383, 1992.

[94] D. F. Price, R. M. More, R. S. Walling, G. Guethlein, R. L. Shepherd, R. E. Stewart, W. E. White, *Absorption of ultrashort laser pulses by solid targets heated rapidly to temperatures 1-1000 eV*, Phys. Rev. Lett. 75, 252 1995.

[95] T. Baeva, S. Gordienko, A. Pukhov, *Theory of high-order harmonic generation in relativistic laser interaction with overdense plasma*, Phys. Rev. E 74, 046404, 2006.

[96] B. Dromey, M. Zepf, A. Gopal, K. Lancaster, M. S. Wei, K. Krushelnick, M. Tatarakis, N. Vakakis, S. Moustaizis, R. Kodama, M. Tampo, C. Stoeckl, R. Clarke, H. Habara, D. Neely, S. Karsch, P. Norreys, *High harmonic generation in the relativistic limit*, Nature Physics 2, 456, 2006.

[97] B. Dromey, S. Kar, C. Bellei, D. C. Carroll, R. J. Clarke, J. S. Green, S. Kneip, K. Markey, S. R. Nagel, P. T. Simpson, L. Willingale, P. McKenna, D. Neely, Z. Najmudin, K. Krushelnick, P. A. Norreys, M. Zepf, *Bright multi-keV harmonic generation from relativistically oscillating plasma surfaces*, Physical Review Letters 99, 085001, 2007.

[98] T. J. M. Boyd, R. Ondarza-Rovira, *Anomalies in universal intensity scaling in ultrarelativistic laser-plasma interactions*, Phys. Rev. Lett. 101, 125004, 2008.

[99] D. A. Serebryakov, E. N. Nerush, I. Y. Kostyukov, *Incoherent synchrotron emission of laser-driven plasma edge*, Physics of Plasmas 22, 123119, 2015.

[100] B. Svedung Wettervik, M. Marklund, A. Gonoskov, *Physics of the laser-plasma interface in the relativistic regime of interaction*, Physics of Plasmas 26, 053101, 2019.